November 2016

Kinetics and dynamics of electrophoretic translocation of polyelectrolytes through nanopores

Harshwardhan Katkar
University of Massachusetts - Amherst

KINETICS AND DYNAMICS OF ELECTROPHORETIC TRANSLOCATION OF POLYELECTROLYTES THROUGH NANOPORES

A Dissertation Presented

by

HARSHWARDHAN HEMANT KATKAR

Submitted to the Graduate School of the
University of Massachusetts Amherst in partial fulfillment
of the requirements for the degree of

DOCTOR OF PHILOSOPHY

September 2016

Department of Chemical Engineering

KINETICS AND DYNAMICS OF ELECTROPHORETIC TRANSLOCATION OF POLYELECTROLYTES THROUGH NANOPORES

A Dissertation Presented

by

HARSHWARDHAN HEMANT KATKAR

Approved as to style and content by:

Murugappan Muthukumar, Chair

Dimitrios Maroudas, Member

T.J. (Lakis) Mountziaris, Member

David Hoagland, Member

John Klier, Department Chair
Department of Chemical Engineering

DEDICATION

In loving memory of my grandparents,

Kusum Katkar and Ramchandra Dongare

ACKNOWLEDGMENTS

I would like to express my sincere gratitude to Professor Murugappan Muthukumar, under whose guidance this work was carried out. I greatly value the experience I have had working with him, and his advice pertaining to research and career. Most importantly, his emphasis on learning, a trait of a good teacher, is sincerely appreciated.

I would like to the members of my dissertation committee, Professors Dimitrios Maroudas, T.J. (Lakis) Mountziaris and David Hoagland, for their detailed suggestions for improving the dissertation. I am also thankful to Prof. Maroudas for his help and advice that, during a time of uncertainty, ascertained the direction of this dissertation.

I am grateful to my friends and colleagues, who made this journey more pleasant than just a journey along the North Pleasant. Finally, I would like to thank my family for their unconditional support and encouragement.

ABSTRACT

KINETICS AND DYNAMICS OF ELECTROPHORETIC TRANSLOCATION OF POLYELECTROLYTES THROUGH NANOPORES

SEPTEMBER 2016

HARSHWARDHAN HEMANT KATKAR

B.Tech., INSTITUTE OF CHEMICAL TECHNOLOGY MUMBAI

M.Tech., INDIAN INSTITUTE OF TECHNOLOGY BOMBAY

Ph.D., UNIVERSITY OF MASSACHUSETTS AMHERST

Directed by: Professor Murugappan Muthukumar

The idea of sequencing a DNA based on single-file translocation of the DNA through nanopores under the action of an electric field has received much attention over the past two decades due to the societal need for low cost and high-throughput sequencing. However, due to the high speed of translocation, interrogating individual bases with an acceptable signal to noise ratio as they traverse the pore has been a major problem. Experimental facts on this phenomenon are rich and the associated phenomenology is yet to be fully understood. This thesis focuses on understanding the underlying principles of polymer translocation, with an emphasis on pore-polymer interactions, polymer architecture, and polymer chain fluctuations. Langevin dynamics simulations are used to study a variety of polymer and pore designs. For a uniformly charged linear polymer, a nanopore with charge patterns along its length is proposed. Variation in the charge pattern length reveals the existence of a critical length at

which the polymer is trapped, causing a significant delay during the pore emptying stage. This trapping is modeled using an appropriate free energy landscape and the Fokker-Planck formalism. The predictions of this theory are in qualitative agreement with the simulation results across different pore and polymer lengths. Moreover, a linear polymer with charge patterns along its backbone passing through such a charge-patterned pore shows rich kinetic behavior; a significant delay is introduced even in the pore entrance and threading stages due to pattern matching, suggesting the use of pore-polymer interactions to slow down translocation. In a related study, the translocation of charged star polymers through an uncharged pore is simulated. Star polymers with different functionalities show rich translocation kinetics while passing through such a pore. The mean translocation time varies non-monotonically with the polymer functionality, suggesting the use of nanopores as a filtering and analytical technique for star polymers.

Recent experiments have suggested the use of phi29 polymerase in conjunction with a protein pore (α-Hemolysin) in the presence of an electric field to slow down the polymer translocation speed, enabling reasonably successful base-calling. The role of polymer chain fluctuations inside the nanopore is evaluated using Langevin dynamics simulations on models of this construct. By monitoring the contributions of the conformational fluctuations of the polymer, the diffusional behavior of monomers of the chain under the speed resulting from the polymerase activity and externally imposed voltage gradients is computed. The simulations show that even if the translocation speed is slowed down considerably by using the polymerase-nanopore construct, the conformational fluctuations of ssDNA inside the pore are always present at high levels, resulting in high levels of noise in the detection signal.

TABLE OF CONTENTS

LIST OF TABLES

Table **Page**

LIST OF FIGURES

Figure **Page**

PERSPECTIVE

Motivation

Transport of charged polymers through nanopores, which includes the transport of genetic materials across nuclear nanopores, is one of the fundamental processes that occurs in a living cell. The transport of the genetic materials, DNA and RNA, through protein pores across the nuclear membrane under the action of electro-chemical potential gradients takes place at very high rates and yet remains extremely selective. The fundamental understanding of the physics behind such a process is yet to be fully developed. Attempts to mimic this translocation process through synthetic or biological pores in a laboratory setup have fallen short due to the lack of good control over the process. Such a laboratory setup is desired because of its applications in separation devices for macromolecules and its potential in DNA sequencing. The motivation behind this thesis is to understand the translocation of charged polymers through nanopores and to evaluate different strategies to achieve better control over the process.

Background

Transport of charged particles through small pores has been used widely in the industry since the inception of the Coulter counter, which is used to measure size of particles suspended in a salt solution. The Coulter counter consists of two compartments containing electrolyte solution connected by a small pore, with one compartment having charged particles. Under the action of externally applied electric field, the charged particles pass through the pore to reach the respective electrodes. The

salt ions cause a certain level of ionic current in a particle-free pore. Particles of different sizes cause different impedance changes when inside the pore; these changes are reflected in the ionic current measured across the pore, making it possible to measure the particle size distributions by performing a statistical analysis of the ionic current.

Identification of either the partial or complete sequence of a DNA is crucial in diagnosing many diseases such as cancer and Alzheimer's disease. Kasianowicz and coauthors [1] have reported one of the first experiments where a setup based on the Coulter counter was used to transport DNA through a nanopore. This experiment demonstrated that the single-file translocation of large DNA molecules through nanopores is possible, and proposed the use of nanopores for DNA sequencing. The working principle is similar to the Coulter counter and is based on the structural differences in nucleotides that results into different changes in the ionic current traces as these nucleotides pass through the pore [2]. Thus, in principle, one could monitor the real-time data for ionic currents as each nucleotide passes through the nanopore during translocation of the DNA and would be able use these ionic current traces to estimate the sequence of the DNA.

However, a key requirement for success of this technique is to enable measurement of the ionic currents at higher rates relative to the rate of translocation. In addition, the inherently stochastic nature of the process limits the accuracy of the ionic current traces. Although this experiment was performed using α-Hemolysin pore, other biological pores (for example, MspA) and solid-state nanopores have also been used in performing translocation experiments [3–5]. Typical speed of translocation in experiments of double stranded DNA through nanopores is of the order of a few nucleotides per microsecond [6, 7]. This speed is too fast to be able to reliably measure the ionic current traces, as the fastest measurement time for the supporting electronics used in experiments today (*e.g.* patch-clamp amplifier) is $\sim O(1\mu\text{s})$. Hence, it is necessary to control the speed of translocation.

Purpose of the thesis

The purpose of this thesis is to develop a fundamental understanding of the translocation of polyelectrolytes through nanopores. Development of such an understanding is required in order to guide the design of the translocation setup for DNA sequencing and to develop newer applications using nanopores. It is of utmost importance to understand the significance of various interactions such as electrostatics and excluded volume between the nanopore and the translocating polymer at a fundamental level, since these interactions can be used to gain the required control over the otherwise highly stochastic translocation process. Additionally, the broader purpose of this thesis is to understand dynamics of the polyelectrolyte chain during its translocation through nanopores.

In the direction of this broader purpose, this thesis focuses on understanding the effects of the characteristics of the nanopore and that of the polymer on the kinetics of translocation. Specifically, the goal of this thesis is to answer the following questions:

- Nanopore characteristics
  - What is the role of electrostatic interactions in translocation kinetics? Can specific charge patterns along the nanopore be used to control translocation kinetics?
  - Can pattern matching between the nanopore and polymer be used to detect a specific sequence along the polymer?
- Polymer characteristics
  - What is the effect of polymer architecture? Is the mechanism of translocation fundamentally different for polymers of different architectures?
  - Can nanopores be used to characterize polymers based on their architecture?

- Modeling polymer translocation
  - What timescales are involved in polymer translocation? Can the conformational fluctuations of the polymer chain inside the nanopore be controlled?
  - Can we use equilibrium theories to describe the process at a fundamental level?

These questions are directly relevant to control of the translocation process as demanded by its applications. They also help to develop an understanding of the basic control parameters that can be used in achieving such a control, and suggest the level up to which control can be achieved.

Thesis organization

The thesis begins with a general introduction of the translocation process in Chapter 1 followed by a brief presentation of the background knowledge of the field available in the literature. Approaches towards modeling the translocation process are discussed and the choice of Fokker-Planck theory is justified. The effective charge of a polyelectrolyte as it translocates across a nanopore is quantified towards the end of the chapter. The role of patterns along the nanopore on kinetics of translocation is discussed in Chapter 2, revealing an interesting pattern matching phenomenon that can be harnessed in characterizing patterned polymers. The system used in this chapter is also used as a model system to demonstrate the use of Fokker-Planck theory. Chapter 3 discusses the effect of polymer architecture on translocation kinetics. Here, a new approach to characterize polymers based on their architectures is demonstrated. Chapter 4 discusses the inherent fluctuations present in translocation of polymers in presence of a pulling motor, and demonstrates the limitations of certain strategies in trying to control the kinetics of translocation. Conclusions based on this work

are discussed in Chapter 5 and an outline suggesting directions for future research is proposed.

CHAPTER 1

POLYMER TRANSLOCATION

Polymer translocation is ubiquitous in nature. It is a fundamental process in cell division in eukaryotic organisms. The replication of DNA inside the nucleus typically requires proteins to translocate into the nucleus from the cytoplasm. On the other hand, after transcription of the genetic information, the messenger RNA translocates from the nucleus into the cytoplasm in order to synthesize proteins. In a typical mammalian cell, this exchange happens across 3000-4000 nuclear pore complexes. In spite of the high exchange rate at which this bi-directional exchange takes place, the process is so meticulously controlled that collisions of translocating materials or congestion of the nuclear pore complexes almost never happens [8].

Developments in our understanding of materials have enabled fabrication of synthetic nanopores, typically made by drilling of Silicon Nitride, Hafnium Oxide, etc. using ion-beam sculpting or electron-beam drilling [9,10]. Naturally occurring nanopores such as MspA and α-Hemolysin pore are also formed in the lab using self-assembly of corresponding proteins. Electrophoresis experiments are performed using these nanopores to study the phenomenon of single-file polymer translocation [1], since these nanopores are narrow enough to prevent any folding of the polymer inside the nanopore. A typical experimental setup used in these experiments consists of two reservoirs containing a salt solution, separated by a membrane embedded with a nanopore (schematic shown in Figure 1.1). Polyelectrolyte is added to the donor reservoir and translocates across the nanopore due to an applied trans-membrane voltage V. Small ions transported due to the resulting electric field towards corre-

sponding electrodes cause a nearly constant level of ionic current across the pore. This ionic current (example shown in Figure 1.2) undergoes a significant drop when the polymer is present inside the nanopore while undergoing translocation. The blocked ionic current can be used to extract enormous information about the polymer. Each polymer chain blocks the ionic current for a certain duration. This information can be used to characterize polymers based on their chain length or chemical identity. The goal is to measure the ionic current with enough accuracy to facilitate the detection of individual nucleotides based on their unique signature in the ionic current. With such an accuracy achieved, nanopores can be used as a low-cost, high-throughput devices for sequencing of DNA.

1.1 Physical insights

A schematic of a polyelectrolyte translocating single-file through a nanopore under the action of an applied trans-membrane voltage is shown in Figure 1.1. The voltage drops significantly only inside the nanopore. However, a weak voltage gradient also exists in the vicinity of the nanopore. Far from the nanopore, the applied trans-membrane voltage is nearly constant. The polyelectrolyte, initially in the bulk of the donor reservoir, has to diffuse from the bulk to a capture region near the nanopore. Once the polyelectrolyte is in this region, it experiences a drift that helps to capture the polyelectrolyte into the nanopore. The capture involves an entropic barrier [11] since the free polyelectrolyte chain loses its conformational entropy as one of its end enters the nanopore. This barrier during capture can be overcome by the forces due to the weak extended electric field, which can be further enhanced by electro-osmotic flow [12] and electrostatic attraction from the nanopore [13]. Nonetheless, the presence of an entropic barrier introduces an inherent stochasticity to the translocation process.

Once the translocation process is nucleated by capturing one end of the polyelectrolyte chain into the nanopore, the electric field compensates for the entropic loss

resulting from the chain losing its entropy as it fills the nanopore. After the nanopore is filled, the rest of the translocation process involves threading of the chain across the nanopore, where for every trailing section of the chain that enters from the donor reservoir, a leading section of the chain comes out of the nanopore into the receiver compartment. This continues until the entire chain disappears from the donor reservoir. Beyond this stage, the polyelectrolyte simply depletes the nanopore and the translocation process is completed.

A nucleated polyelectrolyte chain has a finite probability of translocating successfully across the nanopore instead of being rejected back to the donor reservoir. The translocation process is stochastic in nature also due to the coupled counter-ion dynamics and the kinetics of sticking-unsticking with the nanopore [14, 15]. Moreover, the chain can have different conformations when captured [16, 17], which contributes towards making the process stochastic in nature. Controlling the stochastic nature of the process, however, is a major challenge in devising an experimental system based on this technique.

1.2 Modeling polymer translocation

Translocation of a polyelectrolyte through a nanopore is inherently a complex process. An example of the complex nature of the process is the various suggested scaling laws of the mean translocation time $\langle\tau\rangle$ of a polymer of length N undergoing the translocation process. Sung and Park [18] proposed two regimes of scaling behavior based on the applied potential difference for a polymer undergoing translocation through a hole, assuming the chain friction is dependent on the chain length N. For small favorable trans-membrane voltage, they predicted a scaling of $\langle\tau\rangle \sim N^{(2+\gamma)}$ while for larger driving trans-membrane potential difference, $\langle\tau\rangle \sim N^{(1+\gamma)}$, with $\gamma = 1$ when hydrodynamics can be ignored. Muthukumar [19] used a friction coefficient that is independent of N, and predicted that for a favorable potential difference and for

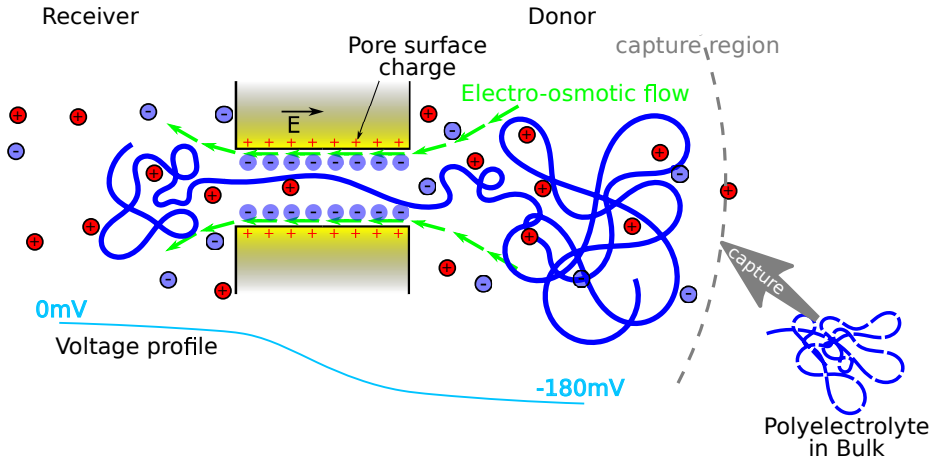

Figure 1.1. Schematic of a typical polyelectrolyte translocation setup. The chain undergoing translocation is shown as a blue curve, while the counter-ions and salt ions are represented using blue (negative) and red (positive) circles. Charges on the nanopore surface (+) can form a double layer causing electro-osmotic flow. The polyelectrolyte chain, initially in the bulk of the donor reservoir (blue dashed curve), is captured into the nanopore with assistance from the electro-osmotic flow and extended electric field due to the trans-membrane potential gradient.

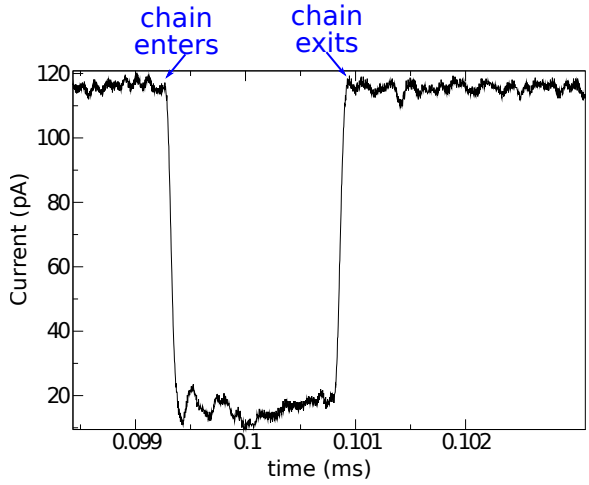

Figure 1.2. A typical ionic current trace showing the signature of a translocation event. The ionic current is blocked as the polyelectrolyte chain enters the nanopore and the open pore current is recovered when the chain exits the nanopore. Data from experiments performed by Byoung-Jin Jeon, University of Massachusetts Amherst (with permission).

longer chains, $\tau \sim N$. For a small electro-chemical potential difference, the scaling $\tau \sim N^2$ is recovered. This scaling relationship was recently observed in Monte Carlo simulation studies of unbiased translocation also by Polson and McCaffrey [20], with modified scaling of $\tau \sim (N - M)^2$ for cylindrical pores of length M. The scaling of $\tau \sim N^{1+\nu}$, with ν being the Flory exponent, was predicted by Kantor and Kardar [21] for a polymer translocating through a hole in the presence of a chemical potential difference assuming that the polymer is in equilibrium at the translocation time scales. de Haan et al. [22] studied non-driven translocation of polymers using Langevin dynamics simulations across a range of pore diameters and found that the scaling exponent α in $\tau \sim N^\alpha$ varies between $2.2 - 3$ with variations in pore diameter. Similarly, in two-dimensional Monte Carlo simulations performed by Luo et al. [23], the scaling exponent α in the scaling equation $\tau \sim N^\alpha$ is found to depend on the pore length and polymer length, for the same applied electric field. The general disagreement in the scaling behavior shows the richness of the phenomenon, emphasizing that making realistic assumptions is crucial in developing a model to describe translocation.

As discussed earlier, the polyelectrolyte chain has to transport from the bulk into the tiny nanopore in order to undergo translocation. To model this phenomenon, the entire process is divided into (a) transport of the polyelectrolyte chain from the bulk into a capture region, followed by (b) capture of the chain into the nanopore and (c) crossing the energy barrier and eventual translocation of the chain across the nanopore [11]. In the bulk, the chain transport is modeled as a combination of drift and diffusion. Major sources of the drift are the applied trans-membrane potential, and any flow that might be induced by pressure difference between the two compartments or by electro-osmotic flow. The chain transport is governed by a steady state convection-diffusion equation that governs the flux of the polyelectrolyte chains into the capture region [11,24]. Once the polyelectrolyte is inside the capture region, which

is assumed to be a hemi-spherical region near the nanopore entrance that is characterized by a capture radius, it is forced towards the nanopore due to a strong drift in step (b). The drift is primarily caused by the extended electric field outside the nanopore entrance and a strong electro-osmotic flow that might be present when the nanopore is charged. The presence of surface charges inside the nanopore gives rise to a surface potential that can be used as a boundary condition for solving the Poisson-Boltzmann equation to estimate the salt concentration profile inside the nanopore. The fluid velocity and hence the strength of the electro-osmotic flow can be predicted for a given salt concentration profile by solving the corresponding Navier-Stokes equation. This model predicts that for high salt concentrations, the velocity profile inside charged cylindrical nanopores is essentially flat and can give rise to strong electro-osmotic flow. If the surface of the nanopore bears a charge that is opposite to the charge of the polyelectrolyte, the resulting electro-osmotic flow is in the direction of translocation. Additionally, velocity gradients in the vicinity of the nanopore cause a transition in the polyelectrolyte chain, from a coil-like conformation in the bulk to a stretched conformation in the capture region. This coil-stretch transition is used to define the capture region, and the required velocity gradient is predicted to be of the order of inverse of the Zimm relaxation time for the polyelectrolyte. For step (c), there is an entropic barrier involved due to the requirement that the translocation has to be nucleated with one end of the polyelectrolyte chain finding the nanopore. When the polyelectrolyte chain is captured, it is typically in a jammed state and has to explore its conformational space until nucleation occurs. This step is slightly different for an α-Hemolysin nanopore due to the specific pore geometry. The vestibule region of the nanopore traps the polyelectrolyte chain. The trapped polyelectrolyte chain undergoes conformational fluctuations while colliding with the vestibule surface until translocation nucleates [25]. The Poisson-Nernst-Planck theory adequately predicts

the two experimentally observed levels of ionic current blockade as the polyelectrolyte chain first enters the vestibule and eventually translocates across the nanopore [26].

The capture radius can be tuned by manipulating the extended electric field and also by the electro-osmotic flow, as seen in the above theoretical discussion. Motivated by this, a lower salt concentration in the donor reservoir with respect to that in the receiver reservoir has been shown to assist capture of the polyelectrolyte. Specifically, the capture rate (number of capture events per unit time) of a DNA into a silicon nitride nanopore is shown to increase by an order of magnitude ($\sim$ 30) for a salt concentration ratio of 20 between the two reservoirs, in comparison with the capture rate for the symmetric salt condition [27]. For α-Hemolysin nanopore, however, this enhancement in the capture rate is shown to be dependent on the trans side (receiver reservoir) salt concentration as well, with lower salt concentration on the trans side causing a non-monotonicity in the capture rate as a function of the cis side (donor reservoir) salt concentration such that the capture rate is maximum at an optimum salt concentration ratio at high pH ($\geq$ 7.5) [13]. An asymmetric pH between the two sides of an α-Hemolysin nanopore is shown to affect the capture significantly, with a two-fold increase in the capture rate as the pH on the trans side of the nanopore is reduced from 7.5 to 4.5 [12]. Furthermore, the reduction in the trans side pH reduces the net negative charge near the trans end of the nanopore, increasing the fraction of events that lead to successful translocation. Although the estimated electro-osmotic flow rate would contribute towards the capture rate, its magnitude is shown to be insignificant in affecting the fraction of events that lead to successful translocations. A combination of pH and asymmetric salt concentrations across the nanopore can be used to further optimize the capture rate, which varies between $0.1\text{s}^{-1}\mu\text{M}^{-1}$ (at a pH of 7.5 and cis, trans salt concentrations of 0.2M, 0.5M) and $400\text{s}^{-1}\mu\text{M}^{-1}$ (at a pH of 4.5 and cis, trans salt concentrations of 0.5M, 2M) [13].

Muthukumar [28] modeled the post-nucleation single-file translocation of a polyelectrolyte chain across a finite length nanopore using a model based on the Fokker-Planck formalism (discussed in Chapter 1.2.1). The model captures many rich aspects of the translocation phenomenon including the presence of an entropic barrier for weak driving forces and the importance of interactions between the nanopore and the polyelectrolyte chain. In presence of the latter, a non-monotonic dependence of mean translocation time on the length of the nanopore is predicted, owing to the competition between the entropic barrier and the pore-polymer interactions. The origin of the pore-polymer interactions can be electrostatic due to surface charges along the nanopore. Motivated by this idea, Forrey and Muthukumar [29] performed coarse-grained Langevin dynamics simulations of a ds-DNA translocating through a cylindrical nanopore using Langevin dynamics simulations to study the role of pore-polymer interactions. By optimizing the cylindrical nanopore size to mimic the essential feature of the α-Hemolysin nanopore (the narrowest constriction), the simulations were able to show that the mode of translocation is predominantly single-file and that hairpin-like conformations do not translocate. More importantly, the essential feature in reproducing experimentally observed event diagram (blockade in ionic current versus event duration) for an α-Hemolysin nanopore was shown to be the presence of charged ring near the receiver end of the nanopore. This result emphasizes the crucial role of surface charge pattern along the nanopore that leads to specific pore-polymer interactions during certain stages of translocation. Experiments based on this idea, involving either site-mutations of the α-Hemolysin nanopore [30] or surface modification of a solid-state nanopore [31] to manipulate the surface charge distribution have shown to be effective in controlling translocation kinetics. The effect of sequences along the polyelectrolyte was studied using the Fokker-Planck model for a di-block copolymer, showing that translocation kinetics are sensitive to the sequences [32]. This theory was extended to the general case of patterns of charges along the poly-

mer chain and verified using Langevin dynamics simulations [33], demonstrating that the sequences along a block polymer can be identified using a nanopore.

The above discussion emphasizes the role of surface charge patterns along the nanopore and the charge patterns along the polyelectrolyte on kinetics of translocation. A systematic study of this role is required and is the focus of Chapter 2.

Translocation of polyelectrolytes is a non-equilibrium phenomenon due to the externally applied electric field. The above discussion also raises an important issue related to the conformation of the polyelectrolyte chain as the translocation process is nucleated. The strong drift present in the capture region can cause the chain to stretch significantly. On the other hand, the entropic barrier during nucleation can allow sufficient time for relaxation of the stretched chain. The fundamental issue of the multiple timescales involved in translocation has led to two distinct approaches towards modeling this phenomenon. If the polyelectrolyte chain is relaxed at the timescale at which it translocates, a quasi-equilibrium assumption can be effective. If, on the other hand, the chain relaxation is not fast enough, non-equilibrium effects have to be taken into consideration. A brief description of the two widely used theoretical approaches that differ with respect to the quasi-equilibrium assumption, the Fokker-Planck model and the tension propagation model, is presented below. The issue of multiple timescales involved in translocation of polyelectrolytes is addressed using Langevin dynamics simulations that help to validate the quasi-equilibrium assumption and the applicability of the Fokker-Planck model used in Chapter 2.

1.2.1 Overview of theoretical models

Figure 1.5 shows experimentally measured mean translocation time $\langle\tau\rangle$ as a function of the polyelectrolyte length N from translocation experiments in the literature [1, 5, 12, 34–38]. An α-Hemolysin nanopore is used in all these experiments (solid-state nanopore in Ref. [5]), with the polyelectrolyte being NaPSS [12, 34, 36],

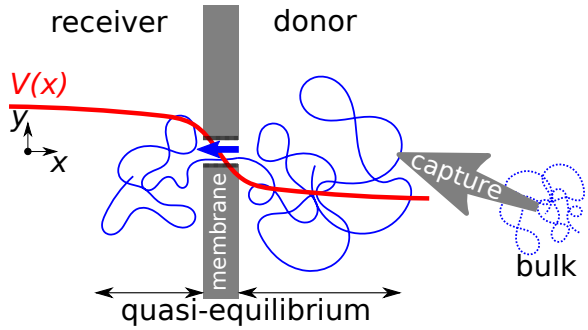

Figure 1.3. Schematic for the translocation setup showing a polyelectrolyte chain (blue) captured from the bulk, followed by its translocation from the donor compartment to the receiver compartment (right to left). A sketch of the trans-membrane voltage profile $V(x)$ extending beyond the nanopore (red curve) that assists in chain capture is also shown. The Fokker-Planck model assumes that the chain is in quasi-equilibrium during the entire translocation.

Dextran Sulfate Sodium [35], ss-DNA [1, 37, 38] or ds-DNA [5]. Multiple data points for a given N correspond to variation in other parameters (trans-membrane voltage [1, 5, 34–36, 38], temperature [37], and pH [12]). The applied trans-membrane voltage V across all these experiments is $40 - 260$mV. The corresponding Zimm relaxation time curve is shown by a solid line. Note that the Zimm relaxation time is calculated using a persistence length of 2nm and a monomer size of 2.5Å and a temperature of 300K. As seen from the figure, a polyelectrolyte chain at equilibrium is believed to relax at a much faster timescale (lower Zimm time) compared to its translocation time for the range of polyelectrolyte lengths used and for typical trans-membrane voltages applied in these studies. Based on these data, a polyelectrolyte chain initially at equilibrium can be assumed to be in quasi-equilibrium as it translocates across the nanopore (Figure 1.3). A one-dimensional free energy landscape can be constructed for the translocation process, using the equilibrium scaling theory for polymers [28, 39] to calculate entropic contribution towards the free energy. This entropic contribution becomes less significant as the trans-membrane voltage increases [15]. Other significant contributions to the free energy are the effective

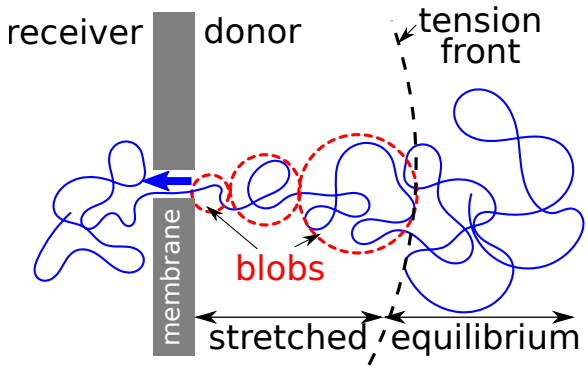

Figure 1.4. Schematic for the two-state tension propagation model. A part of the chain near the nanopore on the donor side is stretched, giving rise to frictional blobs of increasing size. The dotted line shows the tension front that propagates with time to encompass the chain.

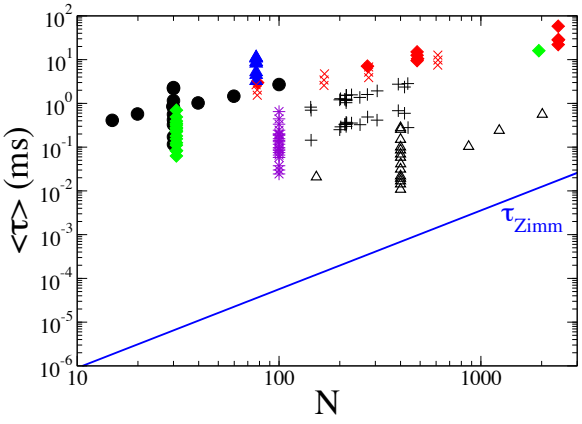

Figure 1.5. Comparison of Zimm relaxation time (blue line) with experimentally measured translocation time (+ [1] △ [5] ▲ [12] × [34] ♦ [35] ♦ [36] • [38] ∗ [37]) as a function of chain length N. Multiple values of $\langle\tau\rangle$ for the same chain length N correspond to variation in other experimental parameters as described in the thesis. A clear separation of translocation and Zimm relaxation timescales is evident for polymers of length up to $N \sim 3000$.

pore-polymer interaction strength, the driving electric field, and the electro-chemical potential difference between the two reservoirs. All experimentally relevant parameters can be taken into consideration while constructing the free energy. Chemical details of the nanopore such as electrostatics and hydrophobicity are modeled using the effective pore-polymer interaction strength, while the salt concentration and pH in the two reservoirs can be accounted for in the entropic contribution. Temperature of the system provides a scale for the free energy. A model based on Fokker-Planck formalism is used to describe the translocation process, with an effective friction coefficient as the only parameter [18, 28]. With the appropriate free energy landscape as an input, the Fokker-Planck equation can predict the mean translocation time and the translocation time distribution (histogram). Excellent agreement with the model prediction is obtained for translocation time histograms from simulations [15] and experiments [40].

For high trans-membrane voltages, however, the quasi-equilibrium assumption can break down and demands an alternative approach. The tension propagation model [41–44] assumes a two-state picture, whereby only a part of the polyelectrolyte chain near the nanopore entrance is stretched during early stages of translocation. The rest of the polyelectrolyte is stationary. The stretching of part of the chain results into formation of blobs of increasing size starting from the nanopore entrance (Figure 1.4). A balance between the driving force and the friction due to formation of blobs gives rise to the dynamic tension propagation equation. The boundary separating the stretched and stationary parts of the chain propagates towards the trailing end according to this equation until it encompasses the entire chain. The reminder of the translocation is assumed to be relatively quick [41, 43]. This gives rise to a time dependent friction coefficient resulting from the stretched part of the polyelectrolyte chain in the donor reservoir, in contrast to a constant effective monomer friction coefficient used in the Fokker-Planck model.

The Fokker-Planck model predicts that for a polyelectrolyte of length N translocating under an applied trans-membrane voltage V, the mean translocation time scales as $\langle\tau\rangle \sim N/V$. Tension propagation model predicts different scaling regimes based on the force due to the trans-membrane voltage: $\langle\tau\rangle \sim N^{2\nu}/V$ for a weak force and $\langle\tau\rangle \sim N^{1+\nu}/V$ for extreme driving force. For intermediate driving forces, the scaling relation is $\langle\tau\rangle \sim N^{\frac{1+3\nu}{2}}/V^{\frac{3\nu-1}{2\nu}}$ if the velocity of the smallest blob is used as a velocity scale for tension propagation [45] otherwise $\langle\tau\rangle \sim N^{1+\nu}/V^{\frac{2\nu-1}{\nu}}$ if the velocity of the largest blob is chosen [16, 46] or if a constant monomer flux is assumed in the stretched chain [43]. Brownian dynamics simulations based on a time dependent friction derived from the tension propagation model [47] show that for short polymers and for narrow nanopores, a significant part of the total friction comes from the friction with the nanopore [48, 49]. In other words the friction of the stretched chain in the donor reservoir is relatively small for narrow nanopores and short polymers and the observed scaling is in agreement with that predicted by the Fokker-Planck model. Moreover, the mean translocation time obtained from simulations scales as $1/V$ for a wide range of the driving force [48, 50]. These simulations predict that the fraction of the total translocation time spent after the tension encompasses the polymer chain is $\sim 0.5 - 0.6$ with chain stiffness reducing it further [51], making the tension propagation stage less relevant for stiffer chains.

Initial polyelectrolyte chain conformations can be far from equilibrium at the onset of translocation because the strong electro-osmotic flow (predicted [24] to be as high as 35cm/s for a typical charge density of 0.14e/nm^2). In addition to creating a strong electric field inside the nanopore, the applied trans-membrane voltage also creates a weak electric field near the nanopore entrance that helps in capturing the polyelectrolyte from the bulk into the nanopore that can cause stretching of the polyelectrolyte chain during capture.

The issue of timescales involved in translocation of polyelectrolytes is addressed in this section by using Langevin dynamics simulations to study translocation kinetics and relaxation dynamics of a polyelectrolyte chain. The effect of chain stretching on the kinetics of translocation is investigated in detail and a comparison of the computed mean translocation time with a characteristic relaxation timescale for these out-of-equilibrium polymer chains is reported.

1.2.2 Simulation methodology

The LAMMPS [52] package is used to perform coarse-grained Langevin dynamics simulations. A set of systematically stretched polyelectrolyte conformations is deliberately generated and subjected to two separate sets of simulations: translocation simulations and relaxation simulations. Details of generating the stretched conformations and the two sets of simulations are given below. Reduced units based on a length-scale of 3Å, energy scale of k_BT and mass scale of 130g/mol are used, unless noted otherwise. k_B is the Boltzmann constant and $T = 300$K is the temperature.

1.2.2.1 Coarse-graining

Details of the simulation setup are similar to those presented in Ref. [15] and are described in Appendix A, with the difference in the choice of length-scale = 3Å and energy scale = k_BT. Briefly, the polyelectrolyte is represented using an array of 120 negatively charged beads of size 1 connected linearly by harmonic springs, with Debye-Hückel electrostatics corresponding to a Debye length of 1.23. For translocation simulations, the cylindrical nanopore and the vertical membrane walls are modeled using stationary uncharged beads and a constant electric field corresponding to the trans-membrane potential V is applied inside the nanopore (Figure 1.8). A time-step of 0.005 is used to integrate the Langevin equation for each polyelectrolyte bead using the velocity-Verlet algorithm.

1.2.2.2 Stretched conformations

The polyelectrolyte chain length in our simulations is kept fixed at $N = 120$. To deliberately generate stretched chain conformations, we adopt a two step strategy. In the first step, an equilibrium polyelectrolyte conformation is generated by simulating a polyelectrolyte chain near a wall for 40000 time units, with one end of the chain fixed near the wall. In the next step, the chain conformation at the end of this simulation is subjected to fluid flow inside a cylindrical channel, with one end of the polyelectrolyte held fixed at a certain location inside the channel. The fluid flowing in the positive x-direction drags the rest polyelectrolyte chain along, generating stretched chain conformations. A set of chain conformations with increasing levels of stretching is generated based on the time that the chain is subject to flow. The above procedure is repeated to generate 500 independent conformations for each level of stretching (Figure 1.6). An average aspect ratio α is used to characterize each set of chain conformations. We define $\alpha = \Delta x/(2r)$ where Δx is the maximum span of the polyelectrolyte chain in the x-direction and r is its maximum radius ($r = \sqrt{y_{\max}^2 + z_{\max}^2}$) from its center of mass (inset of Figure 1.7), averaged over all 500 conformations. We generate systematically stretched sets of conformations using this strategy, characterized by a monotonic increase in α with the time of flow as shown in Figure 1.7.

1.2.2.3 Translocation

The uncharged cylindrical nanopore used for translocation simulations is 16 units long with a radius of 1.8. We choose these dimensions based on geometry of an α-Hemolysin nanopore. Translocation simulations are performed by using a set of 500 conformations corresponding to a given α, nucleating the translocation process by placing one end of the polyelectrolyte just inside the nanopore with the rest in the donor reservoir. A constant electric field equal to $V/16$ is applied inside the

nanopore and the simulation is continued until the polyelectrolyte either retracts back to the donor reservoir (failed translocation) or translocates across the nanopore into the receiver reservoir (successful translocation). Translocation time, defined as the time taken by the polyelectrolyte to exit the nanopore for successful translocations, is measured for 2500 independent simulation runs (5 statistically independent simulation runs per conformation) and averaged to calculate the mean translocation time $\langle\tau\rangle$. Probability of successful translocations is calculated as the fraction of the 2500 runs that lead to successful translocations. The same procedure is repeated for different values of stretching and the trans-membrane potential (α and V). Figure 1.8 shows a snapshot of our simulation setup with two polyelectrolyte conformations corresponding to two distinct levels of stretching (α) at the beginning of translocation simulations.

1.2.2.4 Relaxation

The relaxation simulations are performed in absence of the nanopore and the electric field. Each polyelectrolyte chain with a conformation corresponding to a given α undergoes Langevin dynamics for sufficiently long time (16000 time units) until the initially stretched polyelectrolyte relaxes to an equilibrium shape. An average moment of inertia tensor is calculated from the 2500 independent simulation runs by re-centering each conformation using its center of mass, and average principal moments of inertia λ_i (with $i = 1, 2, 3$) computed from this tensor are used as a metric of relaxation. As a reminder, a conformation corresponding to a shape with one symmetric axis is characterized by two identical moments of inertia ($\lambda_2 = \lambda_3$) and one smaller moment of inertia (λ_1). A spherically symmetric object, such as the conformation of a polyelectrolyte when it is relaxed, has all three principal moments of inertia identical ($\lambda_1 = \lambda_2 = \lambda_3$).

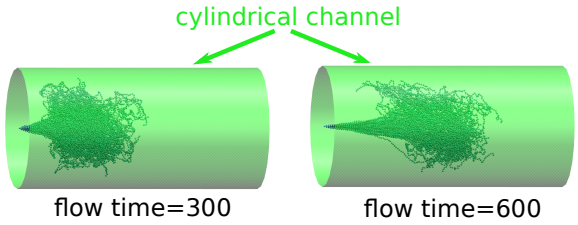

Figure 1.6. Schematic showing systematic stretching of the polyelectrolyte chain conformations when subject to a fluid flow inside a cylindrical channel for short and long time, as indicated, keeping the left chain end fixed. As the chain stretches, it assumes a trumpet-like shape. Each image consists of 500 chain conformations overlaid.

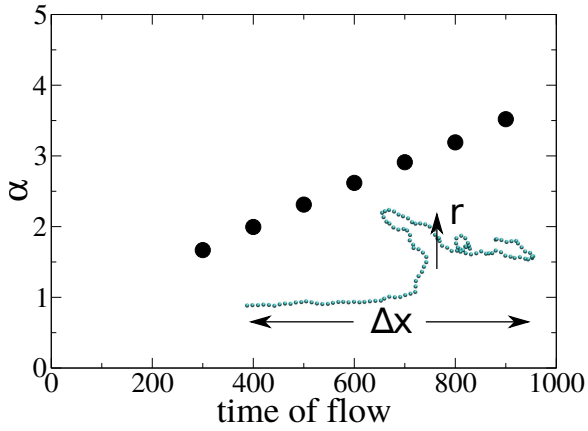

Figure 1.7. Average aspect ratio $\alpha = \Delta x/2r$ of the polyelectrolyte chain as a function of the time for which the chain is subject to flow in the channel. Inset shows definitions of the maximum x-directional span of the chain Δx and its maximum radius r.

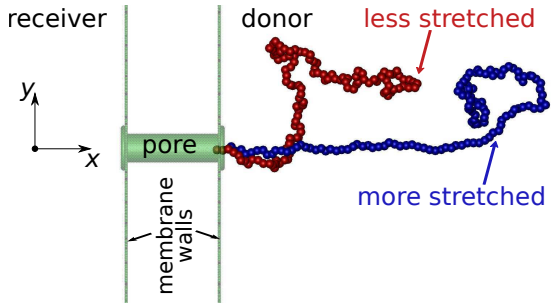

Figure 1.8. Snapshot of the coarse-grained translocation simulation setup with two initial polyelectrolyte chain conformations overlaid. The chain with red beads is less stretched compared to the chain with blue beads.

1.2.3 Results and discussion

The probability of successful translocations obtained from the translocation simulations is plotted in Figure 1.10, as a function of various levels of stretching of the initial conformations α at various trans-membrane voltages V. The mean translocation time $\langle\tau\rangle$ of the polyelectrolyte at various values of α is plotted as a function of the inverse of the trans-membrane voltage V in Figure 1.9. As stretching of the initial conformation of the polyelectrolyte increases, it is more likely to retract back into the donor compartment than to translocate across the nanopore. This is reflected in the probability of successful translocations that decrease with increase in α for all applied voltages. The pull from the initially stretched entropic spring becomes relatively stronger in comparison with the driving electric field, making the probability of successful translocations nearly zero beyond a certain level of stretching for a given voltage (for example, beyond $\alpha = 2.73$ for $V = 0.35$V). This decrease in the probability with increasing α is delayed with increase in the driving trans-membrane voltage. The mean translocation time increases with increase in initial stretching, since the pull from the entropic spring has to be overcome by the applied electric field, causing a delay in the translocation time. However, the increase in $\langle\tau\rangle$ is only moderate across the range of initial stretching studied. A more significant variation in $\langle\tau\rangle$ is observed with respect to the applied trans-membrane voltage. Moreover, a scaling of $\langle\tau\rangle \sim 1/V$ is observed for each level of stretching. The observed scaling is in agreement with the prediction of the Fokker-Planck model, albeit the latter is developed within the quasi-equilibrium assumption. The tension propagation model predicts the same scaling, but only for very weak ($V = 0.0015$V) and very strong ($V = 0.457$V) driving forces [45].

The relaxation simulations performed to study the effect of initial stretching of polyelectrolyte chains on their relaxation behavior show interesting relaxation dynamics. Figure 1.11 shows the trajectories of the three principal moments of inertia

of the polyelectrolyte chain as it undergoes relaxation from the initially stretched state, for different values of initial stretching α. The initially stretched chain is in a trumpet-like shape with one axis of symmetry (Figure 1.6). Hence, at time $t = 0$ the first principal moment λ_1 corresponding to the principal direction along the axis of symmetry of the trumpet is small in comparison with the other two principal moments that are large and nearly equal due to symmetry ($\lambda_2 \sim \lambda_3$). The difference between λ_1 and λ_2 increases with increasing α, since the initial chain conformation is more stretched. As the initially stretched chain relaxes while undergoing Langevin dynamics, λ_1 increases while λ_2 and λ_3 decrease until all three become equal, which corresponds to a spherically symmetric chain conformation.

The mean of the larger principal moments of inertia relative to their value when the chain is completely relaxed is defined as $\langle \Delta\lambda_{2,3} \rangle = \sum_{i=2,3}(\lambda_i(t) - \lambda_i^{\infty})/2$, where λ_i^{∞} is the average value of λ_i for $t > 8000$. We assume an exponentially decaying form $\langle \Delta\lambda_{2,3} \rangle \sim e^{-t/\tau_0}$ to extract the characteristic decay time τ_0. Figure 1.12 shows the trajectory of $\ln(\langle \Delta\lambda_{2,3} \rangle)$ for different values of α. A faster than exponential decay is observed in the initial stages of relaxation of the stretched chain due to quick initial retraction of the polyelectrolyte chain, followed by a systematic exponential decay. Nevertheless, we identify the slope of the linear region in Figure 1.12 as the relaxation timescale τ_0 for the stretched chain and note that this is an overestimate of its true relaxation timescale since the quick initial retraction of the chain is unaccounted for while obtaining τ_0.

A comparison of the mean translocation time from the translocation simulations with the relaxation time τ_0 calculated from the relaxation simulations is shown in Figure 1.13. For all levels of stretching, the relaxation timescale τ_0 is nearly constant. Slight variations in τ_0 are due to the specific time-span used in identifying the linear region in Figure 1.12. The absolute value of τ_0 is only an estimate of the true relaxation time, as discussed above. More important observation is that

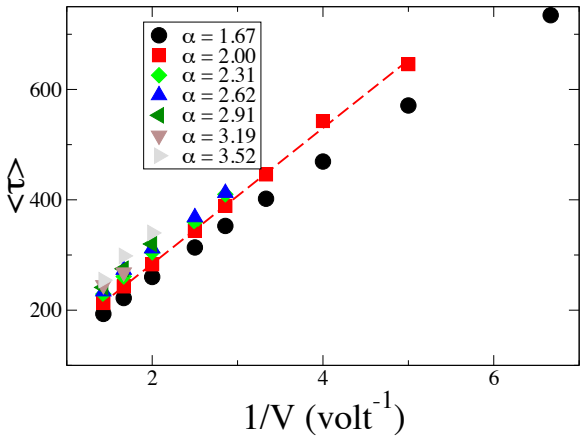

Figure 1.9. Mean translocation time $\langle\tau\rangle$ as a function of trans-membrane voltage V for polyelectrolytes with stretched initial conformations, indicated by α. The dotted red line is shown as a guide to emphasize the observed scaling of $\langle\tau\rangle \sim 1/V$.

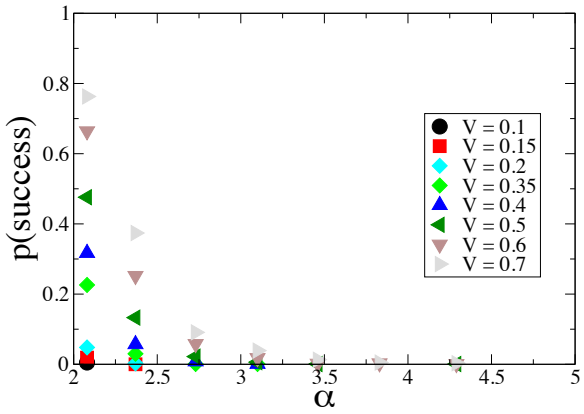

Figure 1.10. Probability of successful translocation for polyelectrolytes as a function of the level of initial stretching α. Legend indicates trans-membrane potential in volts, applied across the 4.8nm long nanopore. Translocation becomes less probable as the initial chain conformation is stretched more.

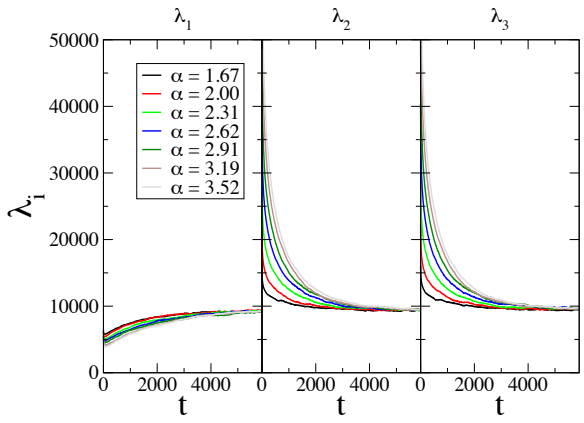

Figure 1.11. The three average principal moments of inertia of the polyelectrolyte chain undergoing relaxation. Legend indicates the initial level of stretching. Initially, the stretched chain has a trumpet-like shape and hence λ_1 (along x-axis) $< \lambda_2 = \lambda_3$ at $t = 0$. As the chain relaxes, the three moments become equal.

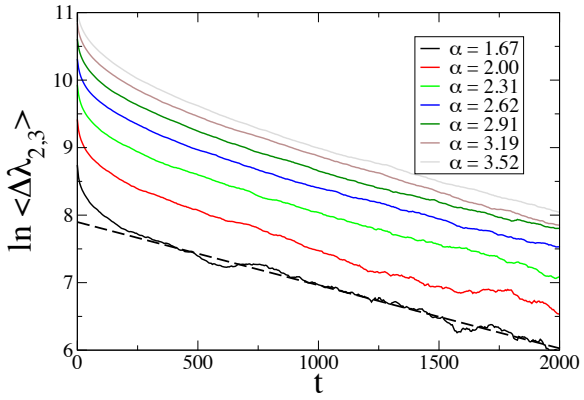

Figure 1.12. A log-linear plot showing the faster than exponential initial decay of λ_2 and λ_3, followed by a systematic exponential decay. We define the average decay $\langle \Delta\lambda_{2,3} \rangle = \sum_{i=2,3}(\lambda_i(t) - \lambda_i^{\infty})/2 \sim e^{-t/\tau_0}$, where λ_i^{∞} is the average value of λ_i for $t > 8000$ and τ_0 is the characteristic decay time. The dotted line is shown as a guide to show the exponential behavior at longer times.

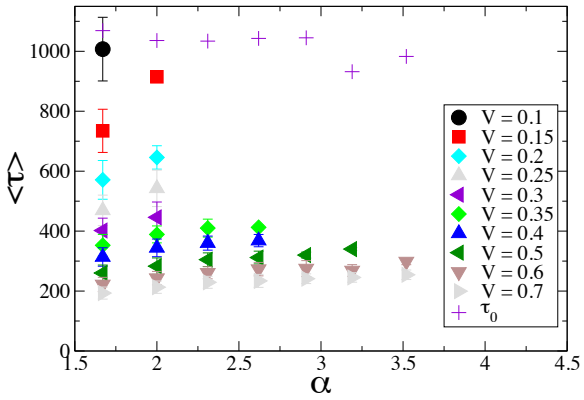

Figure 1.13. Comparison of relaxation timescale τ_0 and translocation time $\langle\tau\rangle$ for stretched polyelectrolytes. Noting that τ_0 is an overestimate of the true relaxation time, the polyelectrolyte chain can be assumed to be in quasi-equilibrium while undergoing translocation.

even the overestimated relaxation timescale is of the same order of magnitude as the mean translocation time for the ranges of initial stretching and the trans-membrane voltage studied. As discussed in Chapter 1.2.1, the trans-membrane voltage applied across a 5nm long α-Hemolysin nanopore in typical experiments is in the range of $0.04 - 0.26$V. Even with the overestimation of the relaxation time, τ_0 and $\langle\tau\rangle$ are quantitatively comparable for the experimentally used trans-membrane voltage range for small initial stretching.

1.2.4 Summary

The results of the above simulations address the fundamental issue of relative timescales for translocation and relaxation and the use of quasi-equilibrium assumption in developing a theoretical description of the translocation process. The two timescales are found to be comparable and the quasi-equilibrium assumption is justified even for the out-of-equilibrium initial chain configurations used in this study, especially for experimentally relevant trans-membrane voltages that are typically less than 300mV across 5nm long nanopores. The deliberate initial stretching of the

polyelectrolyte chain delays the translocation kinetics and makes translocation less probable due to strong retracting force due to entropy.

The Fokker-Planck model has recently been under criticism due to the quasi-equilibrium assumption made in developing this model. Nonetheless, the model is able to describe the rich phenomenology in polymer translocation and is widely used to gain insights into translocation experiments [38, 40, 53]. The results of above simulations establish the validity of this model for experimentally relevant parameter space. We make use of this model to gain insights into our simulation results in Chapter 2.

1.3 Effective charge of a translocating polyelectrolyte

An important parameter that governs the kinetics of driven translocation of a polyelectrolyte chain across a nanopore is the electrophoretic mobility of the chain that determines how fast the chain moves in response to the electric field created by the applied trans-membrane voltage. The electrophoretic mobility of the chain is directly proportional to the number of charges along the chain. In this section, we provide a quick measurement of the effective charge of a polyelectrolyte chain undergoing translocation.

1.3.1 Counter-ion adsorption and confinement

A polyelectrolyte chain releases counter-ions when dissolved in water. However, due to the high charge density along the chain backbone, not all of the counter-ions are free. A certain fraction of the total counter-ions remain adsorbed onto the chain backbone. This fraction can be estimated from the free energy of the system and is an equilibrium quantity, meaning that the free and adsorbed counter-ions are continuously exchanged. Each adsorbed counter-ion decreases the total charge of the polyelectrolyte by an amount equal to the counter-ion's valence. As a result of this,

the effective charge of a polyelectrolyte chain in solution can be lower than the chain's chemical valence. Confinement can further enhance counter-ion adsorption. Due to confinement, the volume available for a free counter-ion is reduced in comparison to the bulk. This reduces its entropic gain upon release and hence shifts the equilibrium such that more counter-ions are adsorbed. Simulations predict that the effective charge of a polyelectrolyte chain confined in an infinite cylindrical channel reduces by a factor of about 3 when the channel radius is decreased from asymptotically large to twice the size of the polyelectrolyte backbone [54]. Such a reduction in the effective charge would reduce the driving force due to electric field and hence the speed of translocation.

While undergoing translocation through a finite length nanopore, a polyelectrolyte chain experiences varying degrees of confinement. To begin with, the polyelectrolyte is in bulk where the free counter-ions have a large volume available. Once captured, it passes through a strongly confined region as it translocates across the nanopore before entering the receiving compartment where it enters bulk again. This change in confinement as the chain translocates leads to a rich counter-ion behavior. Additionally, the small ions consisting of the counter-ions and the salt ions can partition themselves differently between the nanopore and the two reservoirs. Both these phenomena can significantly affect the degree of counter-ion adsorption on the polyelectrolyte chain backbone as it translocates. Thus, the effective charge on the polyelectrolyte is expected to change continuously during translocation. To quantify this, coarse-grained molecular dynamics simulations are performed, taking into account the long-range hydrodynamic and long-range electrostatic interactions. Details of the simulations are discussed next, followed by preliminary results.

1.3.2 Simulations

Coarse-grained molecular dynamics simulations are performed to study the effective charge of a polyelectrolyte chain as a function of its position along the nanopore. A length-scale of 2.5Å, an energy scale of k_BT, with $T = 300$K and a mass scale of 130g/mol are used to derive reduced units. Details of the simulation setup are described in Appendix B. Briefly, the polyelectrolyte is represented as an array of 20 negatively charged beads of size 1 connected linearly by harmonic springs. All the small ions comprising of the counter-ions and salt ions, are represented as beads of size 1. In addition to the 20 counter-ions, small ions corresponding to given salt concentration are explicitly simulated. For a salt concentration of 0.1M, the total number of positive small ions is $32 + 20 = 52$, while the total number of negative small ions is 32. Electrostatic interactions are modeled using a pair-wise Coulomb interaction that is implemented using the particle-particle-particle-mesh algorithm (See Ref. [55] for implementation details). The nanopore is modeled using excluded volume represented by a truncated Lennard-Jones potential at the boundaries. Hydrodynamic interactions are implemented using the multi-particle collision dynamics technique (also known as the stochastic rotation dynamics technique) with parameters chosen to represent a viscosity of 8.7 in reduced units. The simulated box size is $40 \times 40 \times 40$ and the nanopore length is 20, while its radius is varied between 3 and 5. A constant electric field corresponding to a trans-membrane potential of 250mV is applied across the nanopore. Velocity-Verlet algorithm is used to integrate the resulting equation of motion with a time-step of 0.005.

1.3.3 Results and discussion

To expedite the calculations, the translocation process is nucleated with the leading arm of the polyelectrolyte at a distance of 5 inside the nanopore (from the donor side) so that every simulation results into a successful translocation. Under the ac-

tion of the applied electric field, the negatively charged polyelectrolyte translocates along with negatively charged small ions in the direction opposite to the electric field, while most of the positively charged small ions move in the direction of the electric field. The polyelectrolyte chain starts with certain effective charge due to counter-ion adsorption. As the chain translocates, it drags some of these adsorbed counter-ions along with it.

A counter-ion is defined as adsorbed if it is within a distance of 2.0 from the polyelectrolyte, consistent with the definition used in Ref. [54]. The number of adsorbed counter-ions is calculated at every step during our simulations using this definition. The effective degree of ionization is then calculated as the ratio of the number of free ions to the total number of counter-ions. Over 100 independent simulation runs are performed for each set of parameters for statistical averaging, each run beginning with a different equilibrium chain conformation. A binning based on the position of the center-of-mass of the polyelectrolyte chain along the x-direction is performed to calculate the average effective degree of ionization of the chain, α_{eff}, as a function of its center-of-mass position, x_{cm}.

Figure 1.14 shows data obtained from the simulations. A profile of the degree of ionization α_{eff} is shown, as the polyelectrolyte chain translocates, for two different nanopore radii as indicated in the legend. The position of the nanopore is also shown as a guide. The degree of ionization of the polyelectrolyte chain undergoes a dramatic change as it translocates across the nanopore. As the polyelectrolyte enters the strongly confined nanopore region, the effective degree of ionization systematically increases. When the center-of-mass of the chain is at the center of the nanopore, the effective degree of ionization of the chain becomes approximately twice compared to its value in the bulk. This observation is due to the finite length of the nanopore, and is in contrast to the case of a polyelectrolyte confined in an infinite channel [54].

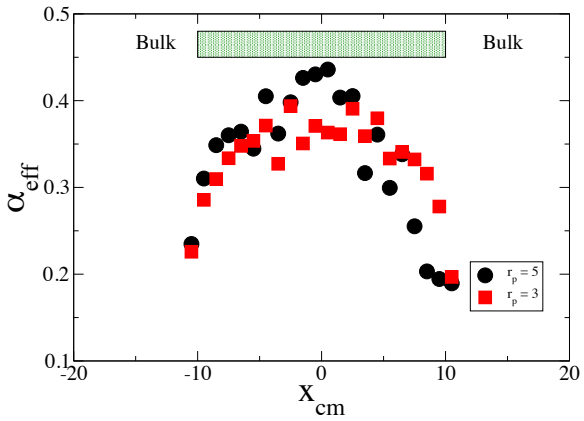

Figure 1.14. Effective degree of ionization of the polyelectrolyte chain α_{eff} as a function of the center-of-mass position of the chain.

Note that in the simulation setup, the electric field is acting only inside the nanopore, while in the donor and receiver compartments, the electric field is zero. Electric field is known to increase the degree of ionization [54], since the counter-ions have a stronger driving force to desorb from the polyelectrolyte. In agreement with this, in our simulations, as larger fraction of the polyelectrolyte chain enters the nanopore, more counter-ions desorb from its backbone, leading to an increase in α_{eff}.

1.3.4 Summary

The effective charge of a polyelectrolyte is computed using molecular dynamics simulations, incorporating the long-range hydrodynamic and long-range electrostatic interactions. Preliminary data shows that the effective degree of ionization of the polyelectrolyte increases as it enters the nanopore and the initial degree of ionization is recovered when the translocation is complete. Detailed simulation study is required to address the role of salt concentration and the identity of the small ions. Additionally, the current simulation methodology can be improved to incorporate the effect of dielectric mismatch between the membrane and the two compartments. A future study in this direction is outlined in Chapter 5. Our preliminary set of simulations

shows that a rich small ion behavior is exhibited in polyelectrolyte translocation, which can be explored in details.

CHAPTER 2

ROLE OF PORE-POLYMER INTERACTIONS

Typical speed of translocation measured in experiments using solid-state nanopores is on the order of $10 - 100$ nanoseconds per nucleotide [6,7]. This speed is too fast to be able to detect the ionic current traces reliably. Hence, it is necessary to slow down translocation. In this chapter, we address the role of charge distributions along the nanopore on the kinetics of translocation of a uniformly charged polyelectrolyte. We also study the effect of charge distributions along the polyelectrolyte on translocation kinetics.

2.1 Review of control strategies for translocation

A few strategies have been suggested in the literature to achieve slower translocation kinetics. Experimentally, equivalent salts of different ionic sizes are found to have different effects on the translocation speed [7]. With longer pores, the interaction between nanopore wall and monomers of the polymer becomes increasingly significant. By introducing a parameter ϵ for the pore-polymer interaction in a model to describe polymer translocation, Muthukumar [28] demonstrated the importance of this pore-polymer interaction on the mean first passage time. In the present context, ϵ is a measure of the strength of the electrostatic attraction between the negatively charged monomers and the positively charged nanopore wall. For large values of ϵ, these interactions become significant even for shorter pores. Two-dimensional Langevin dynamics simulations of a polymer with Lennard-Jones attractive interaction for relatively wide pores by Luo et al. [56] show both a higher success rate and a slower average

time of translocation with increased strength of attractive interactions. Using p and n type dopants, Luan et al. [57] simulated translocation through a nanopore with a p-n junction at the center. The computed electric field is different in the p-doped and n-doped sections, with a reverse electric field at the nanopore center that helps to stretch the polymer. The resulting mean translocation time is also found to be affected due to presence of the two sections.

Effective driving force, defined as the difference between the force due to electric field and the opposing force due to electro-osmotic flow, has been predicted to be dependent on the surface charge density of the nanopore [58]. Ding et al. [59] performed similar numerical electro-hydrodynamic calculations based on the balance between the viscous forces and electric forces that include the effect of surface charge. They found that the surface charge density significantly affects the mean translocation time and suggest the use of surface charges to mediate translocation dynamics. The importance of pore-polymer interactions has also been highlighted in simulations of translocation into a spherical nanopore [60]. He et al. [61] proposed that switching the applied voltage after the DNA capture step can substantially increase the translocation time due to presence of charges along the nanopore walls. The translocation dynamics of a heterogeneous polymer shows rich sequence dependence. The mean translocation time of a multi-block polymer translocating through uncharged pores depends not only on the length of each block [62], but also on the sequence of these blocks [33, 63]. In charged pores [14], an additional dependence is observed on the arrangement of charges along the nanopore walls.

pH is known to protonate charged amino acid residues along protein pore. Wong and Muthukumar [12] studied the effect of pH on translocation of NaPSS through α-Hemolysin and found that, using pH gradient, the charges along the nanopore can be manipulated to increase the probability of successful translocation events. Site-directed mutagenesis can be used to manipulate the charge distribution along protein

pores [30]. Manipulating charges in different regions (both the entrance region and the narrowest constriction) of an α-Hemolysin nanopore is found to change the rate of translocation events significantly. For solid-state nanopores, a pH sensitive coating can be used to tune the charges along the nanopore to control polymer translocation. Both experimentally and theoretically, this has been shown to affect translocation time [31], emphasizing the importance of pore-polymer interactions in the translocation process.

Thus, charge distribution along the nanopore wall seems to have significant effect on the translocation dynamics. In most of the studies so far, however, the pore-polymer interaction is assumed to be constant. Specifically, a uniform charge density is assumed along the nanopore wall. In this work, we investigate the effectiveness of charge distribution along the nanopore wall on translocation dynamics. Keeping the total charge along the nanopore to be constant, we decorate the nanopore with alternate charged and uncharged sections of different lengths. Using Langevin dynamics simulation, we study the translocation dynamics of a uniformly negatively charged flexible polymer through the charge-decorated nanopore. We find that the mean translocation time depends non-monotonically on the length of charged section. The slowest translocation is observed for one particular charge distribution. Numerical calculations based on one dimensional free energy landscape capture the non-monotonic trend observed in simulations. We also study the translocation dynamics of a charge-patterned flexible polymer through the charge-decorated nanopore and find an interesting pattern-matching behavior.

Simulation details are discussed next, followed by the results for translocation time distribution of a uniformly charged polymer translocating through a patterned nanopore. A theoretical framework based on free energy landscape is discussed in Chapter 2.2.2. Simulation results for a patterned polymer translocating through a patterned nanopore are discussed towards the end.

2.2 A uniformly charged polymer translocating through a patterned nanopore

Langevin dynamics simulation of a charged uniform polyelectrolyte undergoing translocation through a partly charged nanopore (with charge patterns) under an applied electric field is performed using the LAMMPS [52] package. A length scale of 12Å is used. This choice is made to reflect the Kuhn length of a flexible polyelectrolyte chain such as the single stranded DNA. We have taken the energy scale as $k_BT/6$, where k_B is the Boltzmann constant, and $T = 300$K is the temperature. Simulation details are given in Appendix A. Briefly, the polyelectrolyte is represented by a bead-spring model made of N beads, with unit negative charge on each bead. A membrane of length M with a cylindrical nanopore of radius $r_p = 1$ is represented by stationary beads along the nanopore walls. The nanopore length is divided into $2N_s$ number of sections, such that beads belonging to odd sections from the nanopore entrance are decorated with a positive charge of $0.1e$, where e is the elementary charge. These sections of the nanopore are, thus, attractive to the negatively charged polyelectrolyte beads. By changing N_s, we can create different charge patterns along the nanopore length, as shown in Figure 2.1. In addition to the excluded volume and harmonic potentials included in the the bead-spring model, the model also accounts for the interaction of the charged polyelectrolyte beads with all other charges through a short-ranged Debye-Hückel potential corresponding to an implicit monovalent salt with a concentration of 0.1M. Further, when inside the pore, each polyelectrolyte bead is acted upon by an electric force, along with additional forces originating from viscous drag and random kicks from the implicit solvent. A time-step of 0.003 is used to integrate the Langevin equation. At the beginning of each simulation run, the translocation process is nucleated by placing one end of the polyelectrolyte chain just inside the nanopore with the rest of the polyelectrolyte beads still in the donor

reservoir. The electric field drives the polyelectrolyte through the nanopore towards the receiving reservoir.

Simulation procedure

An equilibrium polyelectrolyte configuration is required as the initial configuration for the simulation. A polyelectrolyte chain conformation is manually generated and taken as a starting configuration for generating the initial equilibrium configurations. The position of first bead is fixed just inside the nanopore while the rest of polyelectrolyte beads are on the donor side of the pore. The system is then allowed to equilibrate by solving the equation of motion for 10^5 time steps, significantly larger than the Rouse time for the polyelectrolyte chain, with no electric field applied. A velocity-Verlet algorithm is used in LAMMPS to solve the equation of motion.

The polyelectrolyte chain configuration obtained during the last time-step of the equilibration process is taken as an initial equilibrium polyelectrolyte configuration for simulating polyelectrolyte translocation under applied electric field. A uniform electric field $E = 0.43119$ is applied across the pore, with no electric field in the donor and receiver reservoirs. Random velocities with a uniform distribution at the given temperature are assigned to all the polyelectrolyte beads. The equation of motion is then integrated in time using Verlet algorithm until all the polyelectrolyte beads are outside the nanopore on either side. In a successful translocation, the entire polyelectrolyte is translocated to the receiver side of the pore. Translocation time for a successful translocation is calculated as the time at which the last polyelectrolyte bead exits the nanopore on receiver side, starting with the initial configuration of first polyelectrolyte bead just inside the donor end of the pore.

For a given set of parameter values, 2000 runs are performed, almost all of them leading to a successful translocation. The same equilibrated polyelectrolyte chain is taken in each of these runs, with different initial random velocities and random forces

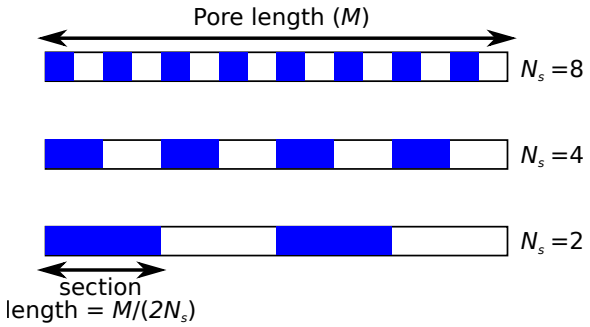

Figure 2.1. Schematic of charge patterns along the nanopore. N_s represents the number of charged sections. Positively charged (blue) and uncharged (white) sections of equal length are placed alternately along the nanopore length.

on the polyelectrolyte beads. We have also performed simulations with 2000 different equilibrium conformations as initial states. The final results are the same as long as the initial chain conformations are equilibrated. A distribution of translocation times for successful translocations is then obtained based on these runs, using which the mean successful translocation time can be computed.

2.2.1 Results and discussion

A nanopore with a total of half the length being charged can be patterned in different ways. In the simplest pattern ($N_s = 1$), the nanopore is divided into two sections, each of length $M/2$, with the first section on the donor side being charged and the second section being uncharged. N_s is the number of pairs of charged and uncharged sections. Yet another pattern ($N_s = 2$) can be formed by having four sections, with each of length $M/4$. In this case, the first and third sections (from the donor side) are charged, while the second and fourth sections are uncharged. In general $2N_s$ number of sections of length $M/(2N_s)$ will have odd numbered sections from the donor side being charged, while even numbered sections are uncharged, with the same total charge in the pore. A schematic of the charge patterns along the nanopore is shown in Figure 2.1. This distribution of charges inside the nanopore significantly affects the translocation process, as observed in the following results.

Polyelectrolyte length	N	60($\times$1.12)
Nanopore length	M	32($\times$1.12)
Debye Hückel cutoff	r_{c2}	3
Debye length	κ^{-1}	0.81
Charge on nanopore beads	α_p	0.1
Electric field	E	0.43119

Table 2.1. Parameter values corresponding to results in Figure 2.2.

Figure 2.2 shows the translocation time distribution for a uniformly charged polyelectrolyte with a chain length $N = 60$ units. The nanopore has alternate charged and uncharged sections, with varying patterns as described above. Each polyelectrolyte bead carries a unit negative charge, while each nanopore bead in the charged sections carries a fractional positive charge of α_p. Thus, charged sections of the nanopore are attractive to the polyelectrolyte. A Debye length corresponding to 0.1M monovalent salt is used for screening electrostatic interactions. The first bead of the polyelectrolyte is placed inside the nanopore to nucleate the translocation process. Under a constant applied electric field inside the pore, the polyelectrolyte undergoes translocation from the donor reservoir to the receiver reservoir. The values of parameters used in obtaining these results are given in Table 2.1. Results using these parameters are shown in Figure 2.2 and are used as a base case for comparison with the rest of the results.

For smaller value of N_s (=1,2), the translocation time follows approximately a normal distribution, with a small standard deviation (not presented). As the number of charged sections N_s increases to 4, the distribution gets skewed, with a longer tail corresponding to a slower translocation as shown in Figure 2.2. The translocation time further increases at $N_s = 8$, with a non-normal distribution having a long exponential tail. However, with any further increase in the number of sections, the translocation time is significantly lower. In other words, all the curves for $N_s > 8$ fall to the left of the histogram for $N_s = 8$. This indicates that slowest translocation occurs at an

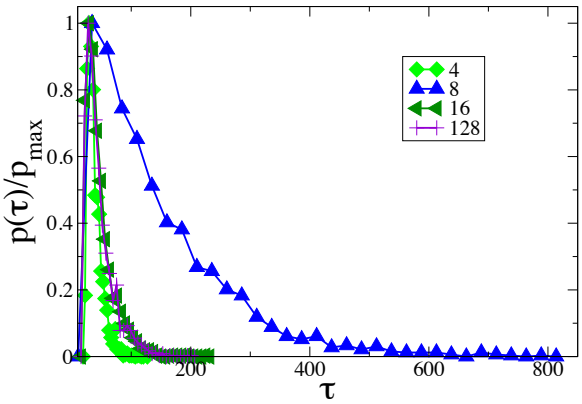

Figure 2.2. Histogram of translocation time, with parameters shown in Table 2.1. Different symbols indicate different numbers of charged sections N_s.

optimum number of sections in a given length of pore, with corresponding optimum in the section length ($L_{\text{opt}} = 2(\times 1.12)$ units).

If the charge on each nanopore bead is reduced to half ($\alpha_p = 0.05$) and the electric field is also halved ($E = 0.215595$), the resulting translocation time distributions show a similar behavior as seen from Figure 2.3(a). A broader translocation time distribution is seen for an optimum length of section ($L_{\text{opt}} = 2(\times 1.12)$ units). The observed optimum disappears with increase in salt concentration. This can be seen from Figure 2.3(b), which corresponds to a salt concentration of 1M. For such a high salt concentration, the charges on the nanopore are considerably screened, thereby reducing the attractive nature of the pore. Hence, the effect of patterns is negligible and the histograms for different patterns almost overlap.

To check if the optimum section length is affected by the cutoff (r_{c2}) used for electrostatic interactions, simulations were performed at a different value of r_{c2} with the rest of the parameters as in Table 2.1 . Figure 2.4(a) shows the resulting histograms for different patterns. It can be seen that the slowest translocation takes place for the same N_s, *i.e.*, charge pattern. Thus, the optimum in section length is not an artifact of the cutoff distance used for electrostatic interactions. Length of the polyelectrolyte

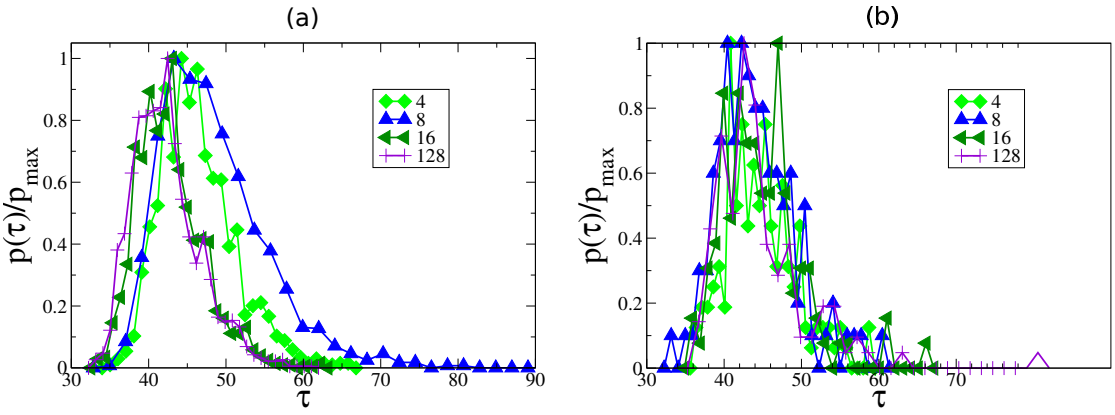

Figure 2.3. Histogram of translocation time with (a) $\alpha_p = 0.05$, $E = 0.215595$ and (b) $\kappa^{-1} = 0.26$ (1M monovalent salt), with the rest of the parameters as shown in Table 2.1. Different symbols indicate different numbers of charged sections N_s.

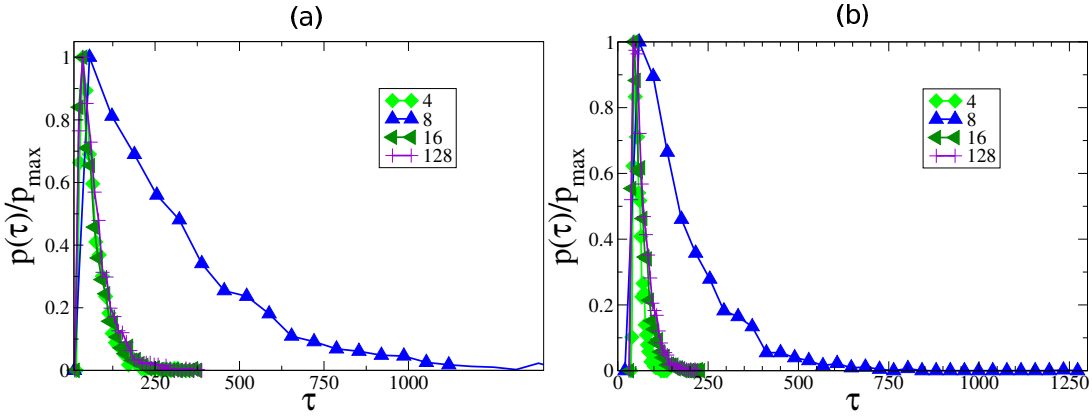

Figure 2.4. Histogram of translocation time with (a) $r_{c2} = 4$ and (b) $N = 120$ and the rest of the parameters as shown in Table 2.1. Different symbols indicate different numbers of charged sections N_s.

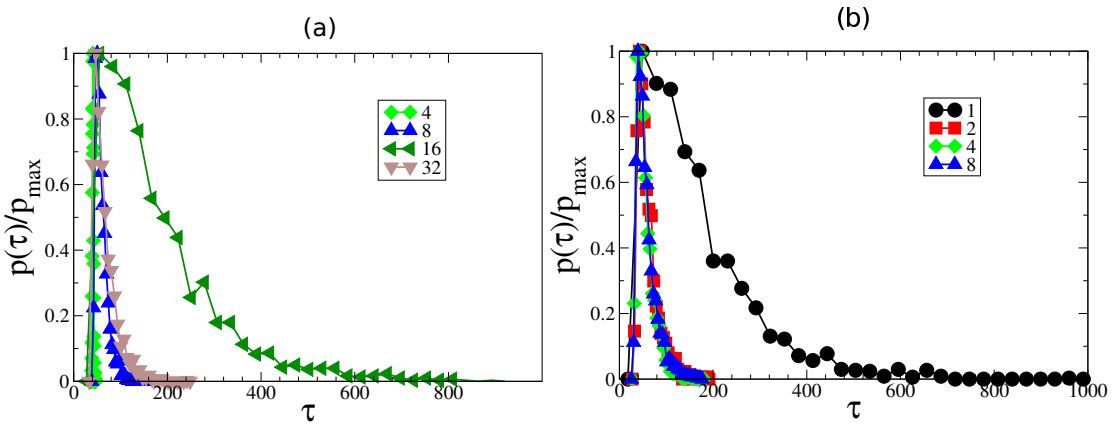

Figure 2.5. Histogram of translocation time with (a) $M = 64$, $N = 120$ and (b) $M = 4$, $N = 60$ with the rest of the parameters as shown in Table 2.1. Different symbols indicate different numbers of charged sections N_s.

chain (N) also does not seem to affect the optimum section length (Figure 2.4(b)). The slowest translocation is observed at the optimum number of sections, $N_s = 8$.

Increase in the nanopore length to twice the value in Table 2.1 results into shift of the optimum number of sections to $N_s = 16$ (Figure 2.5(a)). This clearly indicates that the section length is an important parameter that governs the translocation time distribution. The slowest translocation takes place at a section length of $L_{\rm opt} = 2(\times 1.12)$. This is also verified from Figure 2.5(b), where the nanopore length is equal to twice of $L_{\rm opt}$. The optimum in this case is at $N_s = 1$ which also corresponds to an optimum section length of $L_{\rm opt} = 2(\times 1.12)$.

The average translocation time obtained from the distributions is plotted as a function of length of a section $L_s = M/(2N_s)$ in Figure 2.6. Each curve represents the results obtained with parameters for corresponding figures as indicated in the legend. It can be seen that independent of the values of the parameters studied, the maximum in translocation time, when present, is observed at the same optimum value of $L_{\rm opt} = 2(\times 1.12)$.

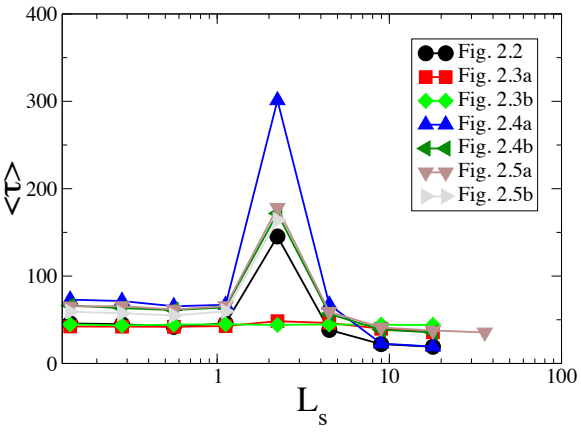

Figure 2.6. Average translocation time as a function of the length of a section $L_s = M/(2N_s)$. Different symbols indicate results with parameters of the corresponding figure.

2.2.2 The Fokker-Planck model

As seen from the results in the previous section, the translocation time distribution is a non-monotonic function of the charge distribution. As we dilute the charges inside the pore, the translocation time first increases and then decreases. This non-monotonicity is universally observed at an optimum charge dilution, independent of the lengths of nanopore and the polyelectrolyte, within the range of parameters studied. To understand this, we consider a polymer of length N, with a charge q_1 on each monomer, translocating under an applied trans-membrane potential difference V_0 through a nanopore of length M with alternate charged and uncharged sections. The process of translocation can be divided into three stages [28]: the nanopore filling stage, the translocation stage and the nanopore emptying stage (Figure 2.7). In each of these stages, the free energy of the system has four major components to it: pore-polymer electrostatic interaction ($F_{\rm ele}$), energy due to externally applied electric field ($F_{\rm ext}$), electro-chemical potential difference between the donor and receiver sides (F_{μ}) and the chain entropy ($F_{\rm ent}$). For a segment of the polymer with $(b-a)$ monomers inside the pore,

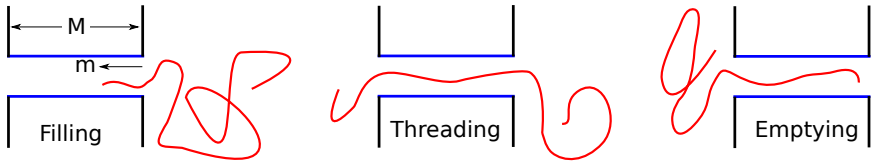

Figure 2.7. Schematic showing the translocation setup along with the three stages of translocation.

$$F_{\text{ele}}(a,b) = N_r \frac{q_1}{4\pi\epsilon\epsilon_0} \sum_{i=a}^{b} \sum_{j=1}^{M} q_2(j) \frac{\exp(-\kappa r(i,j))}{r(i,j)} \tag{2.1}$$

where N_r accounts for interaction between a monomer bead at position i and a ring of N_r nanopore beads at axial position j, $r(i,j)$ is the radial distance between the monomer bead and the nanopore ring and $q_2(j)$ is the nanopore charge at position j along the nanopore axis. Note that the sum over index j is performed taking overlapping nanopore beads into account. The corresponding contribution due to external electric field can be written as

$$F_{\text{ext}}(a,b) = \sum_{x=a}^{b} q_1 V_0 \frac{x}{M}. \tag{2.2}$$

For every monomer that is translocated from the donor reservoir to the receiver reservoir, the electro-chemical potential gradient causes free energy to change by a factor of $\mu = q_1 V_0$. Thus, for x monomers on receiver side, $F_\mu(x) = \mu x$. The entropic contribution for a chain with n monomers on donor(or receiver) side is given from the entropy for a polymer with one end anchored to a wall [19], $F_{\text{ent}}(n) = k_B T(1-\gamma)\ln(n)$. Using these components with appropriate limits, a free energy landscape can be constructed in terms of a translocation coordinate m. For the nanopore filling stage ($0 < m < M$), m monomers are inside the pore, while the rest monomers are on donor side. The free energy of the system is given by

$$F(m) = F_{\text{ele}}(0,m) + F_{\text{ext}}(0,m) + F_{\text{ent}}(N-m). \tag{2.3}$$

In the second stage of translocation ($M < m < N$), M monomers are inside the pore, $N - m$ on the donor side, and the rest on the receiver side. In this stage,

$$F(m) = F_{\text{ele}}(0, M) + F_{\text{ext}}(0, M) + F_{\mu}(m - M) + F_{\text{ent}}(N - m) + F_{\text{ent}}(m - M). \quad (2.4)$$

For the nanopore emptying stage ($N < m < N + M$), $m - M$ monomers are on the receiver side, while the rest are inside the pore. The free energy can be written as

$$F(m) = F_{\text{ele}}(m - N, M) + F_{\text{ext}}(m - N, M) + F_{\mu}(m - M) + F_{\text{ent}}(m - M). \quad (2.5)$$

The contribution of chain entropy F_{ent} is found to be negligible in comparison to other components within the range of parameters used and is ignored henceforth. The probability of finding a state corresponding to the translocation coordinate m at time t is governed by the Fokker-Planck equation [11],

$$\frac{\partial P(m,t)}{\partial t} = \frac{\partial}{\partial m}\left(\frac{k_0}{k_B T}\frac{dF(m)}{dm}P(m,t) + k_0\frac{\partial P(m,t)}{\partial m}\right). \quad (2.6)$$

Here, k_0 is a phenomenological parameter related to the effective friction coefficient per monomer on average. This parameter sets the scale for the time variable in the Fokker-Planck theory. Equation 2.6 can be integrated numerically to get the probability $P(m, t)$, using the appropriate free energy from equations 2.3, 2.4, and 2.5. The probability density for observing the translocation time τ is [11, 64, 65]

$$g(\tau) = -\frac{d}{d\tau}\int_0^{N+M} P(m,\tau)d\tau. \quad (2.7)$$

The derivative of free energy in Equation 2.6 is obtained by using a second order finite difference approximation at internal points and a first order finite difference at the endpoints ($m = 0$ and $m = N + M$). The right hand side of Equation 2.6 is then

discretized using a second order finite difference scheme, with absorbing boundary conditions [11] at $m = 0$ and at $m = N + M$. Numerical integration is performed in Octave using the standard LS-ODE solver. A first order backward difference is used to approximate the derivative in Equation 2.7 to compute the probability density function.

A comparison of the resulting translocation time distribution with that obtained in simulations for a nanopore of length $M = 32$ is shown in Figure 2.8, by taking the phenomenological parameter k_0 as the only fitting parameter. As seen in Figure 2.8, the theory predicts that the slowest translocation time occurs for $N_s = 8$, as in the simulations. The choice of $k_0 = 3125$ in the theory enables the quantitative agreement with simulation results. However, the key result, that the broadest histogram occurring at $N_s = 8$, is independent of the choice for the value of k_0. Similar agreements are borne out for other sets of parameter values used in the present simulations as well. Such a good agreement on the non-monotonic dependence of the translocation histogram on the number of charged sections offers an opportunity to go into the theory, and specifically the free energy landscape, in order to identify the physical reason behind this novel phenomenon.

A typical free energy landscape for the process is shown in Figure 2.9. The translocation process is downhill for the most part along the translocation coordinate, for all charge distributions. However, a free energy well is present towards the end of the nanopore emptying stage (inset of Figure 2.9). This free energy well exists only for a few charge distributions, with varying steepness of the well. The presence of this well results in the long exponential tail observed in the translocation time distribution. This is because the polyelectrolyte gets trapped inside the well and needs to escape the free energy barrier to exit the pore. The trapping of the polyelectrolyte inside the free energy well can be understood as a balance between the driving force due to electric field and the opposing force due to electrostatic attraction with the

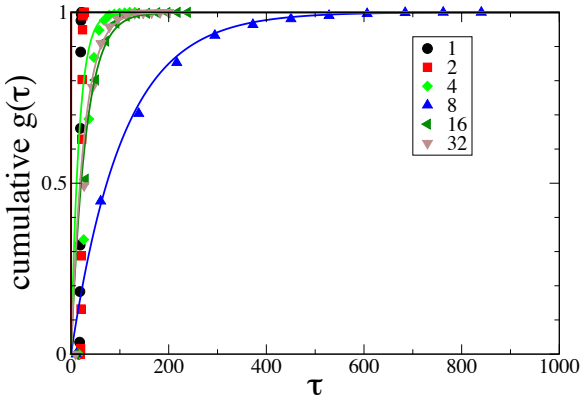

Figure 2.8. Cumulative translocation time distribution for a nanopore of length $M = 32$ and $N = 60$. Symbols represent data obtained from simulations for different numbers of charged sections N_s, while solid lines represent theoretical predictions from Equation 2.7 (for $k_0 = 3125$).

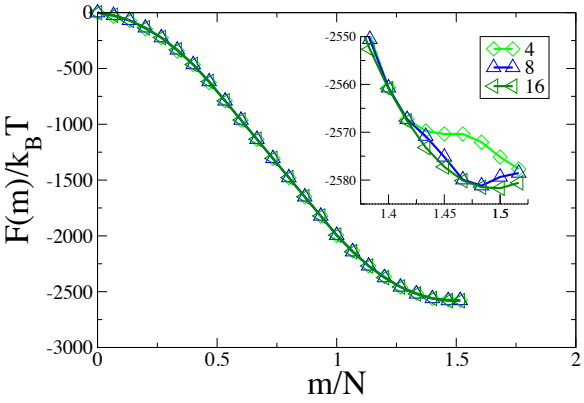

Figure 2.9. Free energy landscape for the translocation of a polymer of length $N = 60$ translocating through a nanopore of length $M = 32$. Inset shows a part of the same data towards the end of translocation process.

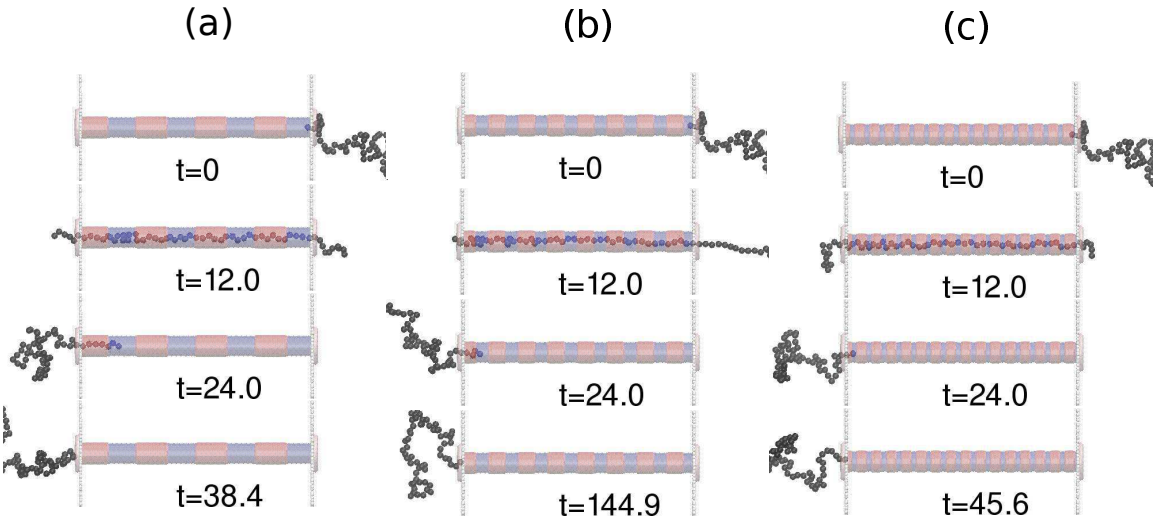

Figure 2.10. Snapshots of simulation at different times. (a) $N_s = 4$, (b) $N_s = 8$ and (c) $N_s = 16$. The chain translocates from the right-hand-side to the left-hand-side.

pore. In the nanopore emptying stage, the number of polyelectrolyte beads inside the nanopore keeps on decreasing. Thus, the total charges inside the nanopore keep on reducing as the nanopore becomes more and more empty, thereby reducing the total force due to electric field. When only a few monomers are present inside the pore, the electric driving force is very weak. Thus, if there are enough charges towards the nanopore end, then the driving force becomes insufficient to overcome the attractive forces. At very low number of charged sections (N_s), the nanopore end is neutral and hence the net attractive forces are weak. However, as N_s increases, more and more charges begin to appear near the nanopore end, resulting in increasing attractive forces. However, at very large values of N_s, even though charges are present near the nanopore end, their concentration towards the nanopore end decreases, thereby reducing the net attractive forces. Thus, only at intermediate values of N_s, the electrostatic attraction of the nanopore is strong enough to cause significant trapping of the polyelectrolyte. Sample snapshots of the simulation at different times are shown in Figure 2.10. It can be clearly seen that for $N_s = 8$, the polyelectrolyte is trapped towards the nanopore end for much longer times.

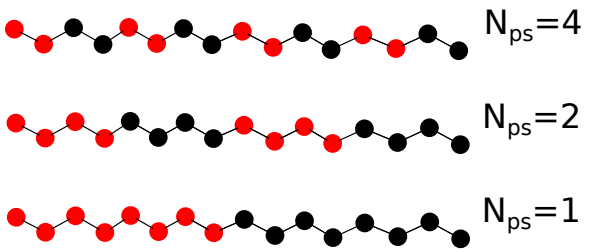

Figure 2.11. Schematic of charge patterns along the polyelectrolyte chain. N_{ps} represents the number of charged sections. Negatively charged (red) and uncharged (black) sections of equal length are placed alternately along the polyelectrolyte chain length N, with section length $= N/(2N_{ps})$.

2.3 A patterned polymer translocating through a patterned nanopore

Translocation of a multi-block polymer through a uniform nanopore has been studied widely [14,33,62,63]. The kinetics of translocation is found to be sensitive to the charge pattern along the polymer. In this section, the kinetics of driven translocation of a charge patterned polyelectrolyte through a charge patterned nanopore is studied using Langevin dynamics simulations.

Simulations are performed using the LAMMPS package. The simulation details are similar to those discussed in Chapter 2.2 with the difference in the model for the polyelectrolyte. The polyelectrolyte chain used in this section is not uniformly charged, but instead is decorated using charge patterns as shown in Figure 2.11. Keeping the total charge on the chain to be constant, its distribution is varied as follows. The total length of the polyelectrolyte $N = 128$ is divided into $2N_{ps}$ sections and only those beads which belong to an alternate section are assigned a charge of $1e$.

2.3.1 Results and discussion

The polyelectrolyte is decorated with patterns represented by the parameter N_{ps} that governs the number of charged sections along its contour length. Additionally,

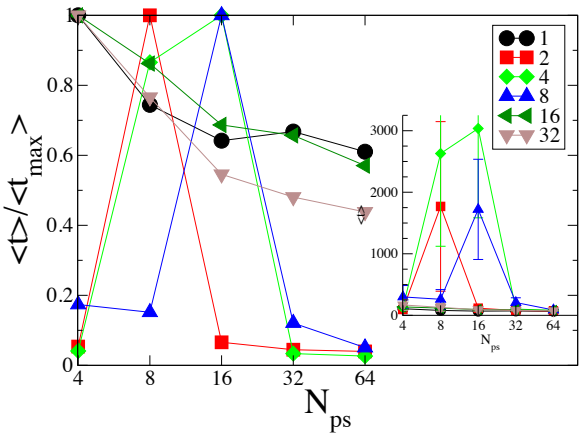

Figure 2.12. Mean translocation time for different patterns along the nanopore and the polyelectrolyte.

the nanopore is decorated with patterns that are represented by the number of charged sections N_s along its length. We vary the values of N_s and N_{ps}, taking care that at least a part of a charged section of the polyelectrolyte is present inside the nanopore during the entire simulation. This is to make sure that the polyelectrolyte is always driven by the electric field.

The translocation process can be divided into three stages: (1) the nanopore filling stage, (2) the threading stage, and (3) the nanopore emptying stage. Figure 2.7 shows a schematic of these stages. In addition to the total translocation time t, we also calculate the time taken by the polyelectrolyte to complete each of these stages. The time taken by the polyelectrolyte to fill the nanopore is denoted by t_1, the time taken for the threading stage is denoted by t_2, while t_3 denotes the time taken for the emptying stage. Figure 2.12 shows the mean total translocation time $\langle t \rangle$, averaged across 100 simulation runs, as a function of N_{ps} for different values of N_s as indicated in the legend. Since the absolute values of $\langle t \rangle$ vary significantly for different patterns (inset of Figure 2.12), the y-axis is rescaled by the largest value of $\langle t \rangle$ for a given pattern N_s on the nanopore. The raw data as well as the rescaled plot clearly highlights the sensitivity of translocation kinetics on the patterns along

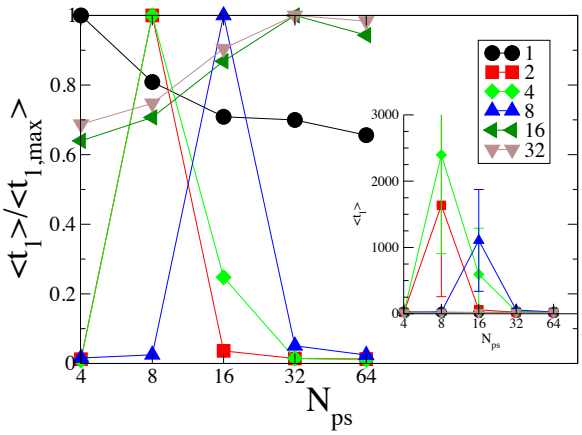

Figure 2.13. Mean nanopore filling time for different patterns along the nanopore and the polyelectrolyte. The mean filling time is rescaled for clarity, with the inset showing the raw data. Different symbols are for different patterns along the nanopore as shown by the legend.

the nanopore and the polyelectrolyte. For example, the mean translocation time for $N_s = 4$ changes by an order of magnitude between various values of N_{ps}.

For a uniformly charged polyelectrolyte translocating through an oppositely charged patterned nanopore, an energy barrier is present in the nanopore emptying stage [15]. The presence of this barrier results into a significant delay in translocation kinetics during the nanopore emptying stage. Even in the absence of any patterns, location of the barrier depends on the nature of the interactions between the nanopore and the polyelectrolyte [11, 28]. For the patterned polyelectrolyte used in the current study, a significant contribution to the total translocation time comes from the nanopore filling and the nanopore emptying stages. Figures 2.13 and 2.14 show the contribution to the total translocation time from the nanopore filling stage $\langle t_1 \rangle$ and the nanopore emptying stage $\langle t_3 \rangle$. The threading stage is the most important stage of translocation for DNA sequencing applications. The mean translocation time for the threading stage $\langle t_2 \rangle$ is shown as a function of the patterns along the polyelectrolyte N_{ps} for various nanopore patterns N_s, in Figure 2.15. The most remarkable result of this work is the strong dependence of $\langle t_2 \rangle$ on the patterns along the nanopore and the polyelec-

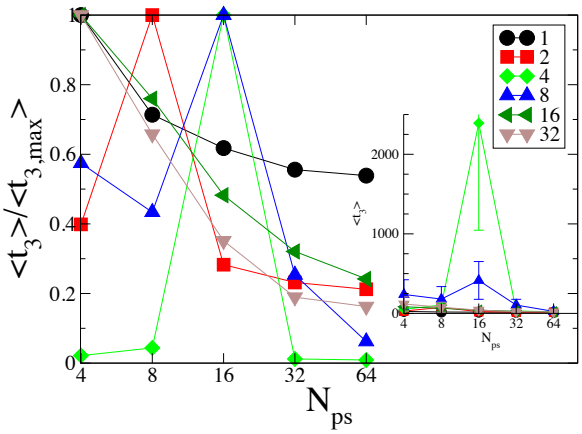

Figure 2.14. Mean nanopore emptying time for different patterns along the nanopore and the polyelectrolyte. The mean emptying time is rescaled for clarity, with the inset showing the raw data. Different symbols are for different patterns along the nanopore as shown by the legend.

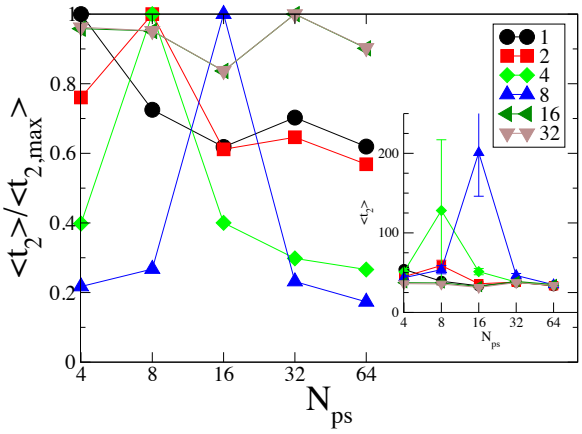

Figure 2.15. Mean threading time for different patterns along the nanopore and the polyelectrolyte.The mean threading time is rescaled for clarity, with the inset showing the raw data. Different symbols are for different patterns along the nanopore as shown by the legend. The combination of charge patterns along the nanopore N_s and those along the polyelectrolyte chain N_{ps} also affect the speed of translocation during the threading stage.

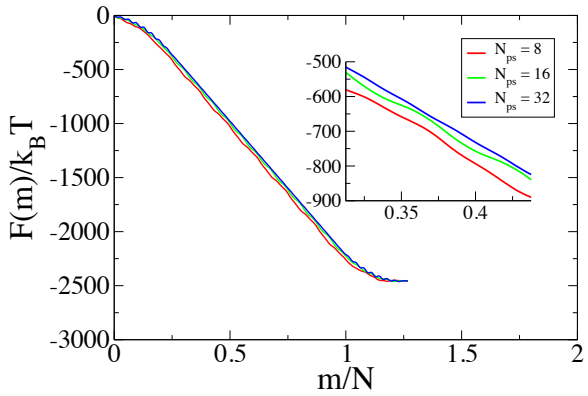

Figure 2.16. Free energy landscape for polyelectrolyte chains with different patterns N_{ps} translocating across a nanopore with patterns corresponding to $N_s = 8$. Inset shows a part of the same data during the threading stage.

trolyte. For example, for a nanopore with $N_s = 8$, there is a five-fold difference in the mean threading time for polyelectrolytes with varying patterns. As discussed earlier, even though the charge distribution along the polyelectrolyte length is different for different values of N_{ps}, the total driving force acting on the polyelectrolyte chain due to electric field during the threading stage is constant across all the charge distributions studied. In other words, the total number of negatively charged polyelectrolyte beads present inside the nanopore is constant during the threading stage. Thus, the dramatic change in the translocation time during the threading stage is due to matching of the charge patterns between the nanopore and the polyelectrolyte. The observed delay in the threading time indicates the presence of energy barriers even in the threading stage. Figure 2.16 shows the free energy landscape for the translocation of polyelectrolytes with different patterns N_{ps} across a nanopore with patterns corresponding to $N_s = 8$. Inset is the free energy profile during the threading stage, showing that the gradient in the free energy is the weakest for $N_{ps} = 16$. Based on the free energy landscape for $N_s = 8$, the slowest threading time τ_2 for this nanopore is predicted for a charge pattern corresponding to $N_{ps} = 16$ along the polyelectrolyte chain, in agreement to the simulation results.

2.4 Summary

We have studied the effect of charge distributions along the nanopore wall on translocation kinetics of a homo-polymer. The translocation is observed to be slowest at an optimum charge distribution, independent of the nanopore and polymer lengths. This is due to the presence of a free energy well near the nanopore end that results in trapping of the polymer. A simple description based on the Fokker-Planck formalism is shown to be able to explain the observed non-monotonic behavior qualitatively.

We have also studied the translocation kinetics of a polyelectrolyte with charge decorations along its backbone, through a charge decorated nanopore. We observe that the translocation kinetics are significantly slowed down for specific combinations of charge patterns along the nanopore and the polyelectrolyte. More importantly, the translocation kinetics are slowed down in all three stages of translocation. Our results are pertinent to the use of nanopores for DNA sequencing applications. Particularly, our results emphasize the role of polyelectrolyte-nanopore interactions on the speed of translocation and can be extended to non-electrostatic interactions as well.

CHAPTER 3

ROLE OF POLYMER ARCHITECTURE

3.1 Star polymers in bulk and in confinement

Polymers with specific architectures find many useful applications. Recent developments in polymer chemistry have enabled synthesis of new polymer architectures such as ring polymers, branched polymers, etc. Star polymers are a subset of branched polymers with only one branch point. These polymers are used in the industry as viscosity modifiers, in manufacturing of adhesives and in optically clear resins [66]. Biological star polymers made of DNA also exist, typically as three arm [67] and as four arm [68] DNA. Recently, star polymers with various functionalities, defined as the number of arms connected at the branch point, have also been synthesized in the lab [69].

Since these polymers are architecturally different from linear polymers, they show different dynamic behavior under various experimental conditions. The mechanism of transport of star polymers is different than the free reptation mechanism by which linear polymers move in concentrated polymer solutions and in gels [70]. For example, in Ref. [71], a linear DNA versus a three arm DNA were compared in terms of their mobilities in polymer solutions. It was found that a linear DNA exhibits a mobility that is independent of polymer concentration in highly concentrated polymer solutions. In contrast, the mobility of a three arm star DNA always depends on the concentration of the polymer solution. While star polymers with higher functionalities result into increasing viscosity of micro-emulsions, linear polymers are found to be more effective in slowing the dynamics of micro-emulsion droplets [72].

On the theoretical front, two different mechanisms have been suggested to understand the transport of star polymers in presence of obstacles such as in a concentrated polymer solution. The reptation mechanism by which linear polymers diffuse in such a system can be extended to star polymers. This extended model assumes that for the center-of-mass of the star polymer to move by a unit length, all but two of its arms have to retract towards its branch point. Such a move would involve an entropic penalty that reduces the diffusion coefficient dramatically, with a multiplicative factor of $\exp(-c_1 N_b)/N_b$ relative to the linear polymer reptation model, where N_b is the number of monomers in each arm and c_1 is a constant related to the entropic potential [73]. A similar exponential dependence is predicted for a three arm star polymer based on the entropic penalty of one arm retracting towards the branch point [74]. A different choice of the potential related to the arm retraction results into a similar scaling with N_b [75]. On the other hand, an alternate mechanism by which a star polymer can diffuse is by dragging all but two of its arms along the direction of motion of the branch point. In other words, the arm ends are not required to retract to the branch point, but are dragged along with it. This mechanism, in combination with reptation, predicts a scaling of $\exp(-c_2 N_b) \times N_b$ for the diffusion coefficient, relative to the linear polymer reptation model [76, 77].

Understanding the behavior of star polymers under confinement has been the focus of various recent studies. This is an interesting problem because the distribution of arms of the star polymer under confinement can lead to rich dynamics and developing such an understanding is required in devising certain applications of interest. For asymmetric star polymers, arm length has been found to have profound effect on transport properties of the polymer in gel electrophoresis [78]. For a three arm star polymer confined in a channel, simulation results reveal that an arm from doubly occupied side of a channel flips side using an equilibrium barrier crossing mechanism [79]. Langevin dynamics simulations show that a four arm star polymer inside a

channel with all arms on the same side of the branch point transitions to the equilibrium configuration of two arms on each side by flipping one arm at a time by forming a loop near the branch point instead of retracting the arm end [80]. In presence of a flowing fluid, conformational dynamics of a star polymer becomes even more important. The critical capture rate of a star polymer into a nanopore is predicted to have a strong dependence on its functionality for certain arm lengths [81, 82]. The star polymer is found to migrate away from the walls of a wide cylindrical pipe due to the flow along the pipe length, with the extent of migration increasing for stars with higher functionalities [83]. Consequently, star polymers with higher functionality flow with a higher average velocity through the cylindrical pipe. These studies, however, are focused on dynamics and equilibrium conformations of star polymers in infinitely long channels. Even in the absence of any confinement, flow of the fluid in the neighboring regions of the star polymer is affected to different extents depending on the functionality of the polymer [84]. Individual arms of the star polymer show a coil-stretch transition similar to linear chains in presence of a fluid undergoing either extensional flow or shear flow [85, 86]. The critical strain rate or critical shear rate at which such a transition occurs, is related to the arm-length instead of the molecular weight of the star polymer. Thus, conformational dynamics of a star polymer are strongly dependent on its functionality.

Translocation of linear polymers through finite-length nanopores itself is a rich problem due to the large number of parameters involved. For example, in the simplest case of charged linear polymers, the charge patterns along the polymer and the pore-polymer interactions play an important role in the translocation kinetics, as seen from simulations [33, 56, 63], experiments [30] and from the theoretical description based on the Fokker-Planck formalism [11, 15]. In experimental work involving DNA translocation, the ionic size of the salt used [7] and the mismatch in salt concentration across the nanopore [13] change the kinetics of translocation. The problem gets even

more complex when polymer architecture is added to the parameter space. For short finite-length pores, hydrodynamic simulations show that the time taken by a star polymer to translocate across the nanopore depends on the initial distribution of the number of arms inside (leading) and outside (trailing) the nanopore [87]. If the translocation process begins with one or more leading arms inside the nanopore, the translocation time is found to increase with increasing number of trailing arms in the initial configuration. On the other hand, increasing number of leading arms beyond small numbers does not affect the translocation time significantly. Note that increasing the number of arms in either case leads to increase in the molecular weight of the star polymer. To arrive at specific conclusions about the role of polymer functionality, a systematic comparison between translocation kinetics of star polymers with varying functionalities but with the same molecular weight is necessary.

In this chapter, we look at the kinetics of translocation of charged star polymers of varying functionalities driven through narrow finite length nanopores. We find a non-monotonic dependence of translocation time on the functionality of the star polymers for a nanopore of given dimensions. The effect of varying the dimensions of the nanopore on the translocation kinetics is also studied. We also comment on the mechanism of translocation of star polymers through nanopores.

Simulation details are described next, followed by the results for kinetics of translocation obtained from these simulations along with a detailed discussion. Key conclusions are summarized at the end of the chapter.

3.2 Simulation methodology

The translocation of star polymers of different functionalities through an uncharged solid-state nanopore under the influence of an electric field is studied using coarse-grained Langevin dynamics simulations. Figure 3.1 shows a schematic of the

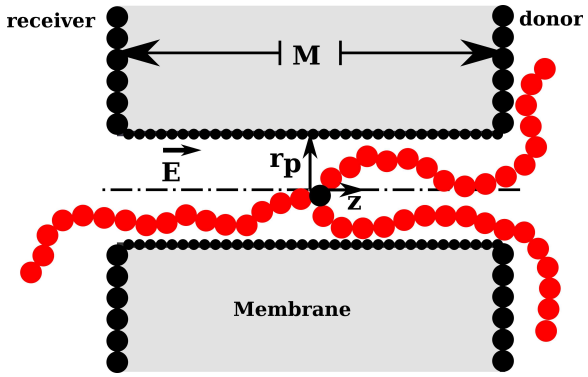

Figure 3.1. Schematic of the simulation setup for a star polymer of functionality $f = 3$. The nanopore is made of static beads shown as black circles. The arms of the star polymer are made of charged beads shown as red circles, connected to a central uncharged bead (branch point) shown as a black circle.

setup. The coarse-grained models for the polymer and the nanopore are explained below.

A bead-spring model is used to represent the star polymer. A spherical bead, connected to other beads using harmonic springs, is used to represent a monomer. The mass and length scales are chosen such that the mass of a monomer bead $m = 1$ (corresponding to a mass of 130g/mol) and size of a monomer bead $\sigma = 1$ (corresponding to a length of 3Å). Independently, we choose the energy scale to be k_BT where k_B is the Boltzmann constant and $T = 300$K is the temperature. All other quantities are converted to reduced units using these scales and are reported in reduced units henceforth, unless noted otherwise.

The total number of monomer beads, $N = 121$, is kept constant across star polymers of different functionalities. f linear arms are connected to a central bead (branch point) to form a star polymer with a functionality f. Consequently, each arm consists of $L_f = (N-1)/f$ beads connected linearly. The branch point is uncharged, while the rest of the beads carry a unit negative charge $q = -1e$ (e is the elementary charge).

The functionality f of the star polymer is varied between 2, 3, 4, 5, 6, 8 and 10. Additionally, a star polymer with a high functionality of 120 is studied. For $f = 120$, however, a slightly different model is used. The uncharged branch point bead is connected to 10 arms, each consisting of 2 beads. The free ends of each of these arms are then connected to 10 beads to form a star-like polymer corresponding to a high f.

The three-dimensional simulation box is divided into two reservoirs, the donor and the receiver, by an M unit thick rigid membrane modeled using two vertical walls. A small hole of radius r_p is present in both the walls and is connected using a cylindrical nanopore of length M. The membrane and nanopore walls are made of immobile and uncharged spherical beads of sizes 1 and 0.25 respectively.

In a typical translocation experiment (Chapter 1), an electric potential difference is applied across the nanopore using electrodes placed in the two reservoirs. The electric potential drops significantly only inside the nanopore. To simulate this in an approximate sense, we set a constant electric field $E = 0.061$ inside the nanopore, acting along the nanopore axis. The electric field is zero in the donor and receiver reservoirs.

Excluded volume between a pair of beads (monomer-monomer or monomer-wall) is modeled using the truncated Lennard-Jones interaction potential (U_{LJ}),

$$U_{\mathrm{LJ}} = \begin{cases} 4\epsilon_{\mathrm{LJ}} \left[\left(\frac{\sigma}{r}\right)^{12} - \left(\frac{\sigma}{r}\right)^{6} \right] + \epsilon_{\mathrm{LJ}} & \text{for } r \leq 1.12\sigma \\ 0 & \text{for } r > 1.12\sigma \end{cases}$$

where ϵ_{LJ} is the depth of the potential well, σ is the mean of the sizes of the two beads and r is the distance between them. Two additional monomer-monomer interactions exist. The springs between bonded monomers are modeled using a pair-wise harmonic bond potential,

$$U_b = K(r - r_0)^2$$

, where $K = 15480$ is the harmonic spring constant, r is the distance between the two connected beads and $r_0 = 1$ is the equilibrium bond length. Electrostatic interactions between monomer beads are modeled using Debye-Hückel potential (U_{DH}),

$$U_{\mathrm{DH}} = \frac{1}{\epsilon_r}\frac{q_1 q_2}{r}\exp(-\kappa r) \tag{3.1}$$

where $\epsilon_r = 80$ is the dielectric constant of the medium, q_1 and q_2 are the charges on the two monomer beads and $\kappa^{-1} = 3.25$ is the Debye length corresponding to a $0.1M$ monovalent salt.

In Langevin dynamics, the above potentials are used to solve the equation of motion for each monomer bead.

$$m\frac{d^2 r}{dt^2} = -\zeta\frac{dr}{dt} - \nabla(U_{\mathrm{LJ}} + U_b + U_{\mathrm{DH}}) + F_r + F_{\mathrm{ext}} \tag{3.2}$$

where r is the position of the monomer bead, t is the time, ∇ is the three dimensional gradient operator and $F_{\mathrm{ext}} = qE$ is the force due to external electric field. The drag force with drag coefficient $\zeta = 1$ and random force F_r acting on the monomer bead due to implicit solvent are related by the fluctuation-dissipation theorem. The above equation is integrated using the velocity-Verlet algorithm implemented in LAMMPS [52] using a time-step of 0.005.

Before setting up the simulation runs, 40 different equilibrium conformations are generated for a given functionality. These equilibrated initial conformations consist of the star polymer with one terminal bead just inside the nanopore and the rest of the beads in the donor reservoir. We comment on this choice of initial conformations in Chapter 3.4.1. For a given functionality f, 2000 independent simulation runs are performed. Each run is started with an initial conformation selected from 40 different

equilibrium conformations generated. In each simulation run, random initial velocities are assigned to all the monomer beads. The equation of motion is then integrated in time until all the beads are on either side of the nanopore. A translocation run is considered to be successful if the entire star polymer translocates across the nanopore into the receiver compartment. Translocation time is define only for successful runs, and is calculated as the time taken by the terminal bead of the last arm to exit the nanopore. The time taken by all the successful runs is averaged to calculate the mean translocation time $\langle\tau\rangle$.

3.3 Results and discussion

A typical simulation run proceeds as follows. As mentioned above, the translocation is nucleated at the beginning of the simulation run by placing one terminal monomer bead belonging to the end of an arm is placed just inside the nanopore entrance. As translocation progresses, more and more beads of the leading arm enter the nanopore. This continues until the branch point is at the nanopore entrance. Depending on the functionality of the star polymer, there can be a delay before the branch point enters the nanopore due to presence of energy barrier associated with simultaneously forcing multiple arms into the nanopore. Once this barrier is overcome, the rest of the arms are dragged along with the branch point into the nanopore. The translocation continues until the rest of the arms exit the nanopore. This closely follows the drag mechanism model proposed in Ref. [76], albeit in presence of a drift. In presence of strong driving forces such as the force due to electric field present in the simulations, the arms of the polymer do not get enough time to retract to the branch point to undergo relaxation. Instead, they are dragged along with the branch point and are compressed inside the nanopore. The free end of each arm enters the nanopore only after the rest of the arm is already inside the nanopore.

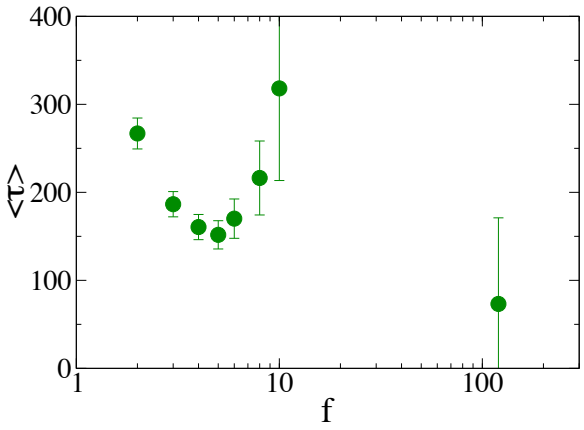

Figure 3.2. Mean translocation time $\langle\tau\rangle$ of star polymers of equal mass as a function of their functionality f for a nanopore of radius $r_p = 3.2$ and length $M = 16$. Note: The polymer with $f = 120$ is used to simulate very large functionality and is architecturally different than other star polymers.

3.3.1 Effect of polymer functionality

In the following, the nanopore dimensions are kept fixed ($M = 16$ and $r_p = 3.2$) to study the translocation of star polymers with different functionalities f. Figure 3.2 shows the mean translocation time $\langle\tau\rangle$ as a function of f. Error bars denote the width of the translocation time distribution. For lower functionalities, the mean translocation time decreases as the functionality of the star polymer increases. This continues until the functionality reaches a critical value, *e.g.*, $f = 6$ for the given nanopore dimensions. Above this functionality, the mean translocation time increases with the functionality. For $f = 120$, however, the mean translocation time is the lowest. As discussed earlier, the star polymer corresponding to $f = 120$ is not strictly similar to other star polymers. Figure 3.2 also shows that the width of the translocation time distribution increases beyond the critical functionality. Figure 3.3 shows the corresponding translocation time distributions. It can be confirmed that for star polymers with functionalities higher than the critical functionality, the translocation time distribution is wider and is characterized by a longer tail. The distribution is narrow and more symmetric for lower functionality star polymers.

These observations can be understood in terms of two competing forces. With increasing functionality, the charge density of the star polymer inside the nanopore increases. As mentioned in the previous section, the translocation is nucleated with one terminal bead of the star polymer inside the nanopore at the beginning of each simulation. Typical translocation event takes place in two parts. In the first part, one arm of the star polymer enters the nanopore and translocates across it. This continues until the branch point of the star polymer is at the nanopore entrance. In the next part, all the remaining arms enter the nanopore together. Thus, during the first part, the charge density is same across different functionalities. In the second part, however, the charge density is higher for polymers with higher number of arms. The length of each arm of the polymer also decreases with increasing functionality. Consequently, the average driving force due to electric field acting on the polymer increases with increasing functionality. On the other hand, increase in charge density leads to swelling of the polymer and hence to an increase in the resistance of the polymer arms to enter the nanopore (confinement). A balance between these two competing forces results into a minimum in the mean translocation time as observed in Figure 3.2. However, for $f = 120$, the driving force is maximum, while the confinement effect is negligible as the nanopore size is larger than the effective size of the particle. Hence, lowest translocation time is observed for $f = 120$.

3.3.2 Effect of nanopore radius

Nanopore radius r_p affects the confinement forces without changing the driving force, and hence changes the results shown in Figure 3.2 significantly. The variation in mean translocation time of star polymers with different functionalities translocating across nanopores of different radii is shown in Figure 3.4. All the features observed for $r_p = 3.2$ (Figure 3.2) are also observed for smaller nanopore radii. The mean translocation time shows a non-monotonic dependence on the functionality of

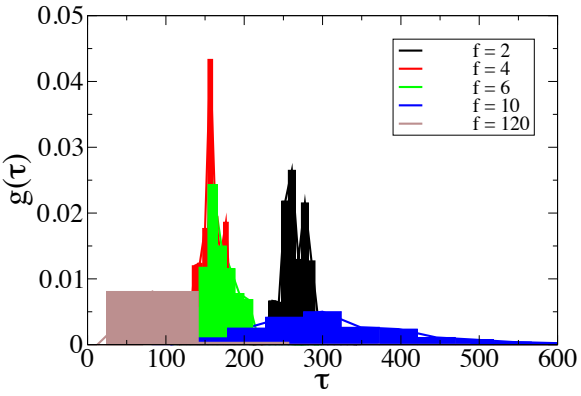

Figure 3.3. Translocation time distribution for polymers with different functionalities f for a nanopore of radius $r_p = 3.2$ and length $M = 16$.

the star polymer. For the lowest functionality star polymer ($f = 2$), narrowing the nanopore does not affect the mean translocation time significantly. For polymers with all other functionalities, the mean translocation time increases with decrease in the nanopore radius. The critical functionality, corresponding to the shortest translocation time, also decreases with decreasing the nanopore radius. Furthermore, a cutoff functionality exists, beyond which any attempted translocation is unsuccessful.

The confinement is negligible for linear polymers ($f = 2$). Hence, nanopore radius does not seem to affect the translocation time for $f = 2$, within the range of nanopore radii studied. For higher functionality polymers, the confinement becomes stronger for smaller nanopore radii, resulting into an increase in the mean translocation time with decreasing nanopore radius. The critical functionality corresponding to the slowest translocation time is a consequence of the balance between the driving force and the opposing force, both governed by the charged density. The critical functionality is found to be affected by the nanopore radius. Additionally, the existence of a cutoff functionality for a given nanopore radius can be explained in terms of the increased strength of confinement for polymers with higher functionalities. These results will be discussed in details in Chapter 3.4.2.

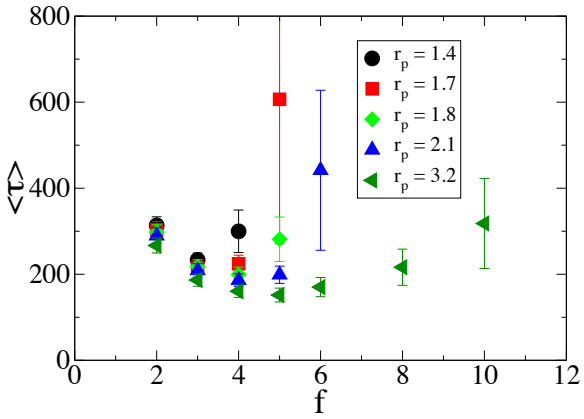

Figure 3.4. Mean translocation time $\langle\tau\rangle$ of star polymers as a function of their functionality f for different nanopore radii r_p. The nanopore length $M = 16$.

3.3.3 Effect of nanopore length

Variation in the nanopore length shows interesting trends in translocation kinetics. The nanopore radius is kept fixed at $r_p = 3.2$, while its length is varied between 2 to 32 units. For systematic comparison, we choose to keep the electric field inside the nanopore to be constant, instead of keeping the electric potential drop across the nanopore to be a constant. The reason behind this choice is that we begin our simulations by nucleating the translocation process with one bead of the polymer just inside the nanopore. The latter option will significantly reduce the driving force during the nanopore filling stage and would also decrease the number of simulation runs that result into a successful translocation.

Figure 3.5 shows the variation in mean translocation time with the nanopore length M. Polymers of different functionalities are denoted using different symbols as indicated in the legend. For a given functionality, the translocation time decreases with increase in the nanopore length for shorter pores. For longer pores, however, the translocation time is independent of the nanopore length. Additionally, we also observe that the sensitivity of translocation kinetics towards functionality of the polymer reduces with increasing nanopore length. Histograms for the translocation time distribution corresponding to three nanopore lengths for different polymer function-

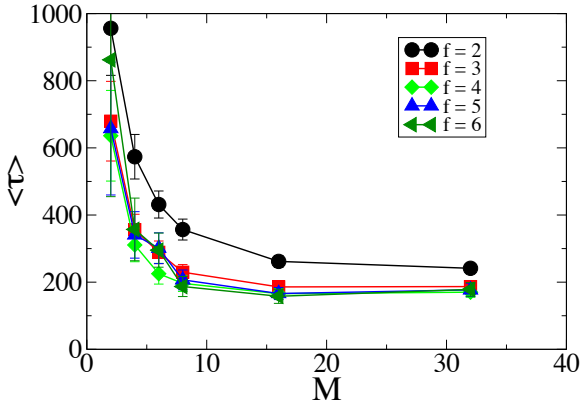

Figure 3.5. Mean translocation time $\langle\tau\rangle$ of star polymers as a function of the nanopore length M. The nanopore radius $r_p = 3.2$. Different symbols indicate different functionalities. Note that the electric field inside the nanopore is kept constant. Hence, longer pores have a stronger driving force.

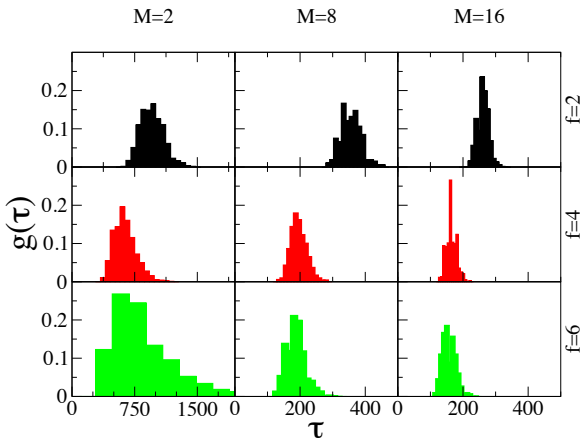

Figure 3.6. Translocation time histograms for star polymers of different functionalities f for different nanopore lengths M. Longer nanopores have a stronger driving force.

alities are shown in Figure 3.6. Histograms for different functionalities have distinct peaks for all nanopore lengths. Additionally, increasing the nanopore length also results into a narrower distribution.

During the nanopore filling stage, each monomer entering the nanopore results into loss of entropy. Longer nanopores can accommodate relatively more monomers inside them, and hence result into a higher entropic loss for the polymer during this stage. Additionally, the resulting larger number of charged monomers inside longer pores result into higher confinement energy and hence into a higher resistance for multiple arms to enter the nanopore. These two effects compete with the increased driving force for longer pores. The observed trends in Figure 3.5 can be understood in terms of these effects. For shorter pores, the energy barrier in nanopore filling stage due to confinement is relatively short. Hence, with slight increase in nanopore length, the increase in the total force due to electric field results into faster mean translocation time. For longer pores, the energy loss due to confinement compensates the gain in the electric field, resulting into a length independent mean translocation time.

Thus, a clear non-monotonic trend exists between the functionality of star polymers and the kinetics of their translocation through uncharged nanopores. Additionally, both the nanopore radius and the nanopore length affect translocation kinetics significantly.

3.4 Insights into the mechanism of transport of star polymers

We now discuss the mechanism of transport of star polymers through nanopores based on the above results. The translocation of a polymer through a nanopore is commonly divided into two steps - polymer capture that involves an end of the polymer finding the nanopore, followed by threading of the polymer across the nanopore. Firstly, we qualify our choice of simulation setup by addressing the issue of multi-

ple arm capture, where ends of two or more arms find the nanopore simultaneously. The observed non-monotonicity is then explained qualitatively in terms of an energy barrier during the threading of the branch point into the nanopore.

3.4.1 One leading arm vs. two leading arms

Diffusion of a star polymer in a melt is significantly slower than its linear counterpart. As discussed in Chapter 3.1, two distinct mechanisms have been proposed in the literature to predict this reduction in diffusion. One mechanism proposes that $f-2$ arms of the star polymer have to retract to the branch point for the center of mass of the polymer to undergo a diffusion step [73]. The timescale for such a retraction is predicted from the entropic penalty based on the probability of having a random walk of length L_f that forms a loop without enclosing any obstacles [74]. An alternate mechanism is where the branch point of the star polymer takes a diffusion step while the trailing $f-1$ arms are dragged along [76]. In this context, we perform simulations to identify the dominant mechanism in transport of a star polymer across a nanopore under the action of an electric field.

As described earlier, we start all our simulations with an end of one of the arms of the star polymer just inside the nanopore. We justify this choice of the initial conformation, in contrast to ends of two or more arms inside the nanopore in the following paragraph.

A significant drop in the applied electric potential takes place across the nanopore, while the potential only weakly changes far from the nanopore. The star polymer has to diffuse to a certain distance near the nanopore, termed as the critical capture radius, before it experiences a drift towards the nanopore due to the electric field. It is entropically unfavorable to have ends of two arms of the star polymer to simultaneously enter the nanopore. Nonetheless, we also simulate this unlikely situation to show that even if this two-arm capture did happen, most of the translocation at-

f	p_{success}
2	0.0742
3	0.0492
4	0.0714
5	0.0554

Table 3.1. Probability of successful translocation, p_{success}, for a star polymer with two leading arms, for various functionalities f of the star polymer.

tempts will fail, resulting into retraction of one or both arms of the star polymer out of the nanopore. For a nanopore with dimensions $r_p = 3.2$ and $M = 16$, our simulations show that less than 10% of events initiated with two leading arms result into successful translocation (see Table 3.1). Such a low probability of success additionally supports our choice of initial conformation. Thus, the diffusion mechanism based on arm dragging [76] is dominant in our system.

3.4.2 Contributions to the mean translocation time

For ease of discussion, consider that the translocation of the star polymer through a nanopore is divided into the following stages defined based on the position of the branch point.

1. Branch point absorption: The branch point approaches and enters the nanopore from the donor reservoir.

2. Trailing arms filling: The branch point is translocated across the nanopore as the trailing $f - 1$ arms fill the nanopore completely.

3. Trailing arms threading: The trailing $f - 1$ arms thread through the nanopore until all trailing arm ends enter the nanopore.

4. Nanopore depletion: Ends of the $f - 1$ arms translocate across the nanopore and exit the nanopore.

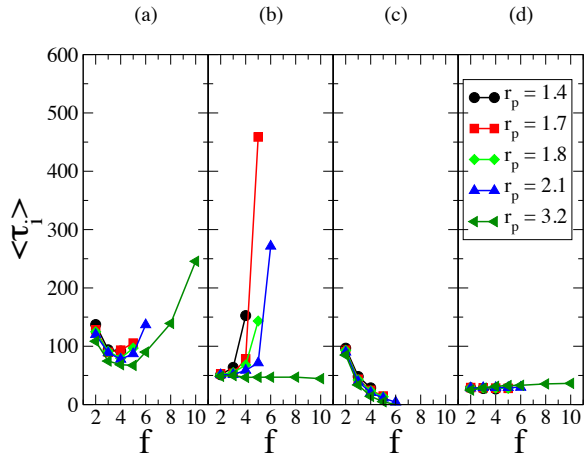

Figure 3.7. Detailed time taken for each stage of the translocation, for different nanopore radii corresponding to Figure 3.4. Average time for (a) Branch point absorption τ_1 (b) Trailing arms filling τ_2, (c) Trailing arms threading τ_3 and (d) Nanopore depletion τ_4 is plotted for star polymers of functionality f and nanopore radii r_p.

We compute the average time taken for the above stages based on successful simulation runs and denote these by $\langle\tau_1\rangle$, $\langle\tau_2\rangle$, $\langle\tau_3\rangle$ and $\langle\tau_4\rangle$ respectively. Figure 3.7 shows the average time taken for each of these stages.

A rich phenomenology clearly exists in the translocation process. To understand the contributions from each of these stages to the total translocation time, we discuss different competing effects below.

3.4.2.1 Path length and Driving force

In our system, the length of each arm of the star polymer L_f decreases as its functionality increases. Thus, for example, a linear polymer has the longest contour length from end to end ($= 2L_f = 120$), compared to the contour length from end of the leading arm to the end of a trailing arm for a three arm star polymer ($= 80$). Assuming single-file translocation, the total path that the polymer needs to travel while undergoing translocation, thus, decreases with increasing functionality. This effect alone would cause the mean translocation time to decrease with increasing functionality of the star polymer.

Except for the first stage of translocation, the driving force due to electric field increases with increasing functionality of the star polymer. This is an effect of the increased linear monomer density inside the nanopore which by itself would cause the mean translocation time to decrease with increasing functionality of the star polymer.

3.4.2.2 Confinement

For a given nanopore radius, once the branch point is captured, the trailing arms of the star polymer have to enter the nanopore. The entropy of the star polymer reduces as more of the nanopore is filled by the trailing arms. Moreover, the strong electrostatic repulsion between monomers of the trailing arms causes an energy penalty for having multiple arms filling the nanopore. This effect alone would increase the mean translocation time with increasing functionality of the star polymer.

When the branch point completes threading, the situation is different because beyond this time, the number of monomers belonging to the trailing arms that enter the nanopore from the donor reservoir is the same as those that come out of the nanopore on the receiver reservoir. We expect this effect alone to lead to a behavior similar to the path length effect.

3.4.3 Phenomenology of star polymer translocation

The observed trends in Figure 3.7 can be explained in terms of the above effects. Firstly, the time taken for the nanopore depletion stage $\langle \tau_4 \rangle$ is not sensitive to the functionality of the star polymer or the nanopore radius. During this stage, both confinement and the driving electric force act synergistically to drive the polymer out of the nanopore.

The translocation velocity during the trailing arms threading stage is nearly constant for different functionality star polymers as seen from a plot of the average time taken for this stage as a function of the arm-length L_f in Figure 3.8. Thus, the path length effect causes $\langle \tau_3 \rangle$ to decrease with f. Moreover, the velocity slightly increases

as the nanopore radius increases since the arms are slightly less stretched in a wider nanopore. This reduction in stretching is evident from the fact that the time taken for trailing arms threading through a $r_p = 3.2$ radius nanopore, $\langle \tau_3 \rangle \sim 0$ for the star polymer with functionality $f = 6$ (the corresponding arm length is 20), even when the nanopore length $M = 16$.

The average time taken for the branch point threading stage $\langle \tau_2 \rangle$, during which the nanopore is gradually filled by all the trailing arms, increases with the number of trailing arms and hence the star functionality. For a star polymer of a given functionality, $\langle \tau_2 \rangle$ decreases with increasing nanopore radius. The time taken for this stage is governed by the balance between the entropic and electrostatic penalty of putting monomers of the trailing arm into the confined nanopore, and the increase in driving force due to increased charges while doing so. For the narrow nanopores, the entropic and electrostatic penalty dominates and causes the average time of this stage to increase with f. However, for the widest nanopore ($r_p = 3.2$), the entropic and energetic penalty is insufficient to cause such an increase.

In our simulations, the star polymer experiences the presence of the membrane wall right from the beginning of each run. For lower functionality star polymers, the path length effect dominates, causing the average time for the first stage $\langle \tau_1 \rangle$ to decrease with increasing f. However, as the number of trailing arms increases, the average time increases due the presence of the wall, delaying the translocation process.

3.5 Summary

We have studied the translocation of charged star polymers of varying functionalities through an uncharged nanopore, driven by electric field. The key observation made in this thesis is the strong dependence of the mean translocation time on the functionality of the star polymer. Moreover, this dependence is non-monotonic, with

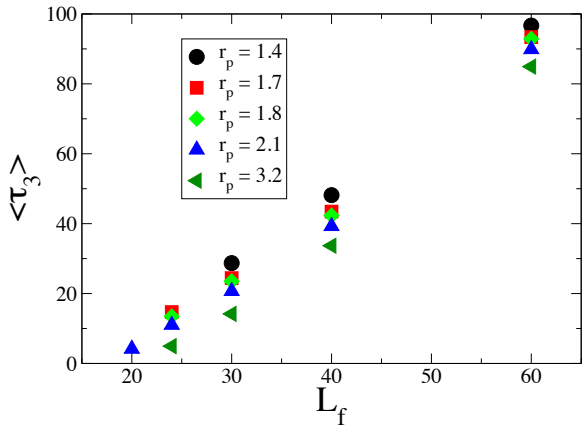

Figure 3.8. Average time for the trailing arms filling stage $< \tau_3 >$ for star polymers of different functionalities, plotted versus the star polymer arm length $L_f = 120/f$.

the presence of a minimum for a particular functionality. This minimum can be shifted by changing the dimensions of the nanopore.

Gel electrophoresis is used as an analytical method for detecting and isolating star polymers based on their architecture. However, such techniques have limited sensitivities and are indirect in the sense that one can only distinguish between polymers based on their sizes. Our study shows that the translocation time histograms (which can be measured experimentally) of architecturally different polymers translocating through nanopores are clearly distinguishable with distinct peaks for certain nanopore dimensions. This suggests that nanopores can be used as an alternative analytical tool for detection and separation of charged polymers based on their architecture.

Although our study is based on charged polymers, the results are general as long as the driving force increases with the functionality of the polymer. For instance, neutral semi-flexible polymers can be distinguished by dragging them through nanopores using fluid flow. Such a simulation study would require incorporating hydrodynamics in the simulation model. The dimensions of the nanopore can be fine-tuned to further improve the distinguishability. Additionally, the pore-polymer interactions can be used to further optimize such a device. These parametric studies are required to be

studied in details in the future. Nonetheless, the results of this chapter are promising as a proof of concept.

CHAPTER 4

ROLE OF POLYMER CHAIN FLUCTUATIONS

4.1 Polymer translocation using motor protein

An interesting approach has been recently proposed to control the kinetics of electrophoretic translocation of DNA through commonly used biological nanopores [3, 4]. This approach is based on the idea of using phi29 DNA polymerase as a motor protein. phi29 is a DNA polymerase that replicates a template single stranded DNA by synthesizing a complementary strand. The phi29 polymerase has an active polymerization site where the complementary strand is synthesized. It also has an exonuclease site for hydrolyzing erroneous nucleotides from the complementary strand for accurate replication. The average rate of replication is on the order of 40 nucleotides per second, well within the desired range for DNA sequencing applications. This rate is found to decrease when tension is applied on the the template strand [88]. In this recently proposed approach, the phi29 polymerase is complexed with a single stranded DNA. A primer strand and a blocking oligomer are attached to the DNA such that the activity of phi29 polymerase is suppressed in the bulk due to the presence of the blocking oligomer. External electric field drives this entire complex towards the nanopore, with the template DNA threaded into the nanopore, followed by gradual unzipping of the blocking oligomer. The phi29 polymerase gets activated due to this strategic unzipping of the blocking oligomer and starts exerting a motor force on the template DNA. An externally applied electric field and the motor force due to the phi29 polymerase act in opposite directions, resulting into controlled translocation kinetics. Although the resulting reduction in translocation speed is in the desired range,

the question about readability of the corresponding ionic current traces needs to be addressed. With the aid of Langevin dynamics simulations, we study the dynamics of different segments of the DNA inside the nanopore, in response to a hypothesized two-step mechanism by which the motor forces act. The motivation behind this work is to validate the effectiveness of this new approach in reliably detecting nucleotide sequences from the ionic current traces. The two-step mechanism that we hypothesize is qualitatively similar to the power-stroke model proposed in the literature for protein translocation [89, 90]. The structure of phi29 polymerase also suggests a two-step mechanism where a complementary nucleotide has to diffuse to the active site and then bind to the complimentary DNA strand, followed by relative displacement of the DNA [91].

4.2 Model and simulation methods

Reduced units are derived for all quantities using the scales for three fundamental quantities: mass=130g/mol, length=3Å and energy=k_BT, where k_B is the Boltzmann constant and $T = 300$K is the temperature. All values reported in the rest of this chapter are in reduced units, unless explicitly stated.

The simulation setup (Figure 4.1) consists of a thick membrane that divides the simulated region into two compartments. The membrane is embedded with a MspA nanopore with the nanopore axis aligned in the z-direction. The nanopore is oriented such that the nanopore entrance (vestibule region) is on the right hand side. In other words, the left and right compartments are on trans and cis side of the nanopore. A phi29 polymerase complexed with a ss-DNA is placed near the nanopore entrance on the right and oriented such that its tunnel corresponding to the ss-DNA is along the nanopore entrance.

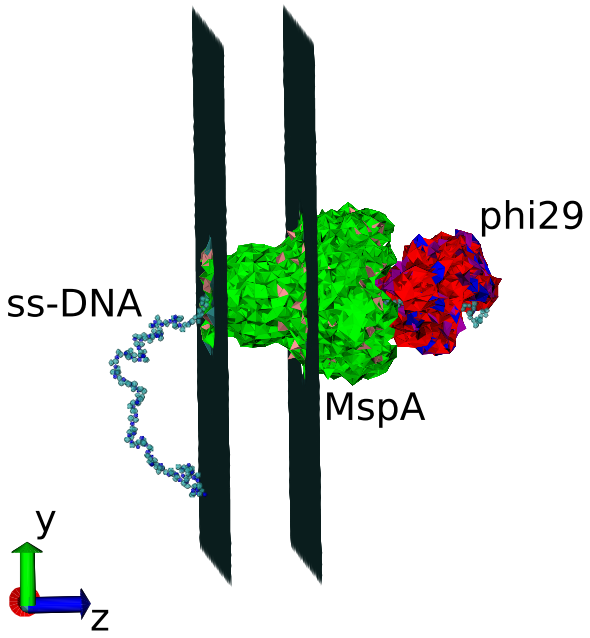

Figure 4.1. A typical snapshot of the simulation setup. Pore and polymerase beads are shown as polyhedra for visualization. The phi29 polymerase pulls the DNA chain in the positive z-direction (to the right), while the opposing force due to the electric field is along the negative z-direction. The resulting motion of the DNA is towards the right.

4.2.1 Coarse-graining

The membrane is represented by two parallel walls made from spherical beads of size 1.8 arranged in a rectangular array. We use X-ray crystal structures of the MspA nanopore [92] and the phi29 polymerase [91] from the protein data bank to obtain corresponding coarse-grained models. In these coarse-grained models, each residue of the MspA nanopore and the phi29 polymerase is represented by a united-atom bead with diameter 1 unit, with the center at the C-α position. Each coarse-grained bead is assigned charge corresponding to physiological conditions. Thus, the beads corresponding to ARG, HIS and LYS residues are assigned a unit positive charge, while those corresponding to ASP and GLU residues carry a unit negative charge. Rest of the beads are neutral. Coordinates obtained after coarse-graining are then translated and rotated as required to generate the simulation setup.

The origin is chosen at the entrance of the MspA nanopore, with the z-direction along the nanopore axis. The membrane walls are located at $z = -29.5$ and $z = -14.8$, the MspA nanopore extends from $z = -31.17$ to $z = 0$, and the phi29 polymerase extends from $z = -3.5$ to $z = 17.92$.

The ss-DNA consists of 100 nucleotides and is initially placed such that 64 nucleotides are in the trans compartment, while the rest are either inside the MspA nanopore, inside the phi29 polymerase or in the cis compartment. Each nucleotide is represented using a three-bead model, with spherical beads of diameter 0.83 corresponding to a base, sugar and a phosphate group. Each phosphate bead in a nucleotide belonging to the ss-DNA is assigned a unit negative charge while the sugar and base beads are neutral. We number the beads starting from the cis side, such that the base, sugar, and the phosphate beads of the first nucleotide are numbered 1, 2 and 3 respectively. Thus, the entire ss-DNA is made using using 300 beads.

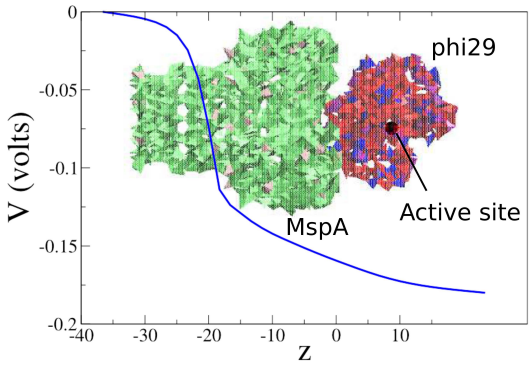

Figure 4.2. Voltage profile inside the nanopore. The approximate locations of the MspA nanopore and the phi29 polymerase are also shown. The active site of the phi29 polymerase is marked with a black circle.

4.2.2 Voltage profile

A potential difference of 180mV is applied across the membrane. The negatively charged ss-DNA experiences a force towards the trans side due to electric field, against the direction of the pulling force due to motor protein. The resulting voltage profile across the nanopore is obtained by solving the Poisson-Nernst-Planck equation (Equation 4.1) in absence of the DNA, using the boundary conditions that the electric potential is equal to 0mV at the left boundary and is equal to -180mV at the right boundary.

$$\begin{aligned} \epsilon_0 \nabla . [\epsilon(\mathbf{r}) \nabla \psi(\mathbf{r}, t)] &= -\sum_i z_i e c_i(\mathbf{r}, t) - \rho_{\text{pore}}(\mathbf{r}) \\ \frac{\partial c_i(\mathbf{r}, t)}{\partial t} &= \nabla \cdot [D_i \nabla c_i(\mathbf{r}, t) + \mu_i c_i(\mathbf{r}, t) \nabla \psi(\mathbf{r}, t)] \\ \mu_i &= \frac{z_i e D_i}{k_B T} \end{aligned} \tag{4.1}$$

Here, ϵ_0, k_B, and e correspond to permittivity of free space, Boltzmann constant, and elementary charge, respectively. The dielectric constant $\epsilon(\mathbf{r})$ varies depending on

whether the location $\mathbf{r}$ is in the protein or in the rest of the region containing water. We choose $\epsilon = 2$ for the protein and $\epsilon = 80$ for water. The salt is assumed to be potassium chloride, with concentration of the monovalent ($z_i = \pm 1$) potassium and chloride ions to be 0.3M at the simulation boundaries. The diffusion coefficients D_i for potassium and chloride ions are $0.196\text{Å}^2/\text{ps}$ and $0.203\text{Å}^2/\text{ps}$, respectively [93]. The above set of coupled equations is solved numerically for the given charge distribution ρ_{pore} inside the MspA nanopore and the phi29 polymerase, to get the resulting salt concentration profile $c_i(\mathbf{r}, t)$ and the electric potential profile $\psi(\mathbf{r}, t)$ at steady state (as discussed in Ref. [11]). Figure 4.2 shows the resulting voltage profile, with the MspA nanopore and phi29 polymerase positions shown as a guide.

4.2.3 Driving forces

The beads corresponding to MspA nanopore and phi29 polymerase are kept fixed at their positions throughout the simulation. The beads corresponding to the ss-DNA interact amongst themselves and with the nanopore, polymerase and membrane beads according to the following pair-wise interactions.

Excluded volume and electrostatic interactions between two beads i and j with charges q_i and q_j, separated by a distance r, are modelled using a truncated Lennard-Jones potential (U_{LJ}) and a Debye-Hückel potential (U_{DH}) respectively. These potentials are given by the following equations.

$$U_{\text{LJ}} = \begin{cases} 4\epsilon_{\text{LJ}} \left[\left(\frac{\sigma}{r}\right)^{12} - \left(\frac{\sigma}{r}\right)^{6} \right] + \epsilon_{\text{LJ}} & \text{for } r \leq 1.12\sigma \\ 0 & \text{for } r > 1.12\sigma \end{cases} \tag{4.2}$$

$$U_{\text{DH}} = \frac{C q_i q_j}{\epsilon} \frac{\exp(-\kappa r)}{r} \qquad \text{for } r \leq r_{c2} \tag{4.3}$$

Here, $\epsilon_{\text{LJ}} = 1$ is the depth of the truncated Lennard-Jones potential, while σ is the average of the sizes of the two beads. The Debye length is $\kappa^{-1} = 1.873$, corresponding to a monovalent salt concentration of 0.3M; a choice made to mimic the experimental

conditions used in Ref. [4]. The constant $C = 1$ in reduced units. The Lennard-Jones potential is truncated at the distance where the potential is minimum. This preserves only the repulsive part of the potential. A size is assigned to each bead by choosing the appropriate value of σ. For example, $\sigma = 1$ for a phi29 polymerase bead. The Debye-Hückel potential is truncated beyond the cutoff distance of 3 for computational efficiency.

The beads belonging to ss-DNA have an additional harmonic bond potential interaction U_b to represent bond connectivity and an angle potential U_a to restrict the angle θ between the base, sugar and phosphate beads, given as follows.

$$U_b = K(r - r_0)^2 \tag{4.4}$$

$$U_a = K_a(\cos(\theta) - \cos(\theta_0))^2 \tag{4.5}$$

The spring constant $K = 2580$ and the angle energy constant $K_a = 125$, while $\theta_0 = 65^\circ$ is the base-sugar-phosphate equilibrium angle. These potentials along with the chosen parameter values are used to represent the DNA as a semi-flexible chain.

The position r of each bead belonging to the ss-DNA is updated using the equation of motion given by,

$$m\frac{d^2r}{dt^2} = -\zeta\frac{dr}{dt} - \nabla(U_{\mathrm{LJ}} + U_{\mathrm{DH}} + U_b + U_a) + F_r + F_{\mathrm{ext}}. \tag{4.6}$$

Here, $m = 1$ is the mass of the bead, t is the time and $\zeta = 50.5$ is the bead friction coefficient. ∇ is the three dimensional gradient operator. The random force F_r is related to the friction coefficient by the fluctuation dissipation theorem [11]. The external force F_{ext} has two contributions to it: the contribution due to the electric field and the contribution due to the pulling force of the motor protein. The above

equation of motion is integrated using the velocity Verlet algorithm implemented in LAMMPS [52], using a time-step of 0.005.

The electric field acts only along the z-direction and is calculated from the voltage gradient shown in Figure 4.2. The pulling force of the motor protein acts on the ss-DNA bead nearest to the location (2.165,-1.565,7.818). In the reminder of this chapter, we refer to this location as the active site. Figure 4.2 also shows the location of the active site.

4.2.4 Procedure

The phi29 polymerase is known to synthesize a complimentary DNA strand at a typical rate of synthesis of 40 nucleotides per second [88]. To mimic the polymerase activity, we adopt the pull-relax strategy in our simulations. At $t = 0$, the ss-DNA bead nearest to the active site is rapidly pulled towards the active site in 5 simulation steps, which corresponds to 0.054ps. This bead is then held at the active site for t_{relax} simulation steps. The nearly instantaneous displacement created during the pulling stage travels along the ss-DNA chain during this relaxation stage. In this work, we study the dynamics of beads at different locations along the ss-DNA chain for $t_{\text{relax}} = 10^6$ steps, as discussed in Chapter 4.3. Positions of all the beads are stored after every 5 steps for computational efficiency.

4.3 Results

The starting configuration is such that the 23rd bead (corresponding to sugar of the 8th nucleotide) along the ss-DNA chain happens to be present nearest to the active site. We denote the position of a ss-DNA bead from the chain end on the right side by s, while the bead pulled at the active site is denoted by s_0. As explained earlier, after pulling this bead at the active site ($s_0 = 23$), we let the chain relax for t_{relax} steps before pulling the next sugar bead towards the active site, *i.e.* $s_0 = 26$.

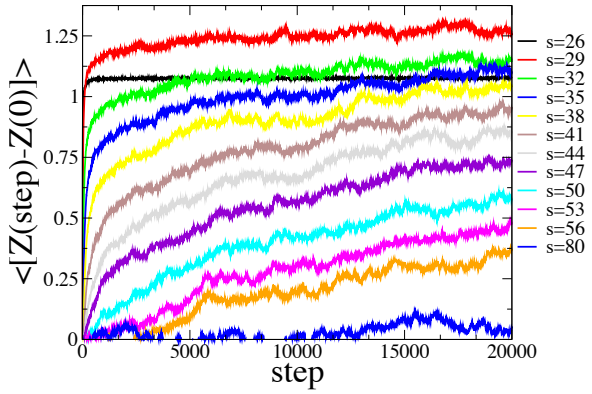

Figure 4.3. Trajectories of marked sugar beads s in z-direction. Different colors represent data for different marked beads, as indicated in the legend. For this set of trajectories, 26th bead is pulled towards the active site ($s_0 = 26$). This bead reaches the maximum displacement quickly, as seen from the trajectory in black color. The neighboring beads catch up, but with a lag.

The choice of specifically pulling a sugar bead is arbitrary and is a consequence of the chosen starting configuration. We continue these pull-relax stages for all the sugar beads along the backbone of the ss-DNA.

Figure 4.3 shows the displacement in z-direction of marked ss-DNA beads s for $s_0 = 26$, averaged across 79 independent simulation runs, for $t_{\text{relax}} \equiv 10^6$ steps. The displacement calculations are limited up to 20000 steps for computational efficiency. The values of t_{pull} and t_{relax} used in the simulations correspond to a motor protein that acts faster than the typical rate of synthesis of the phi29 polymerase (40nt/s) by a factor of 2×10^6. However, as seen in Figure 4.3, the ss-DNA chain is relaxed at a much shorter time, well within the chosen value of t_{relax}. The choice of t_{relax} is thus justified, since we are interested in the dynamics of the ss-DNA chain as it relaxes.

As seen from Figure 4.3, the bead pulled towards the active site ($s_0 = 26$) quickly undergoes displacement in z-direction and then remains at the active site for rest of the relaxation steps. The next bead ($s = 29$) along the ss-DNA backbone follows its displacement with an associated delay, as shown by the red curve. This continues for all consecutive beads with an increasing delay. At the same time, the maximum

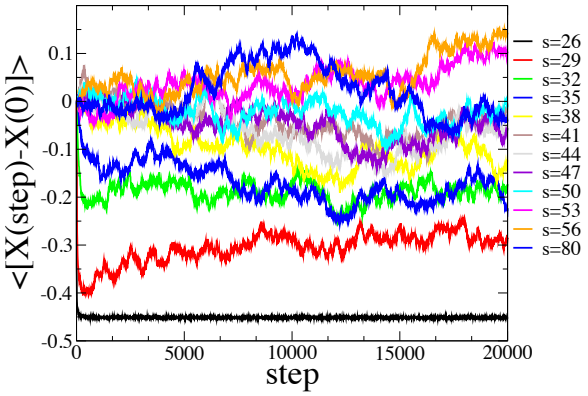

Figure 4.4. Trajectories of marked sugar beads s in x-direction. Different colors represent data for different marked beads, as indicated in the legend. For this set of trajectories, 26th bead is pulled towards the active site ($s_0 = 26$). The pulled bead reaches the maximum displacement quickly, as seen from the trajectory in black color. The displacement of the neighboring beads is only slightly related to that of bead 26 and the correlation is absent beyond a few consecutive beads.

displacement that a bead undergoes also decreases for consecutive beads along the ss-DNA backbone.

Figure 4.4 shows corresponding trajectories in x-direction (for $s_0 = 26$). Similar to the displacement in z-direction, bead 26 of the ss-DNA undergoes maximum displacement instantaneously and then fluctuates around the same mean position. Note that unlike the displacement in z-direction that always takes place in the positive z-direction, the x-directional displacement of the ss-DNA bead at the active site is governed by the geometry of the channel near the active site of the phi29 polymerase. Thus, in Figure 4.4, bead 26 has an average negative displacement due to the location of the active site. In contrast to the displacement in z-direction, the x-directional displacement of the next sugar bead of the ss-DNA ($s = 29$) is only slightly related to that of bead 26. All the consecutive beads along the ss-DNA chain undergo random fluctuations around an average. Hence, the net drift in the x-direction is nearly zero for the rest of the beads downstream.

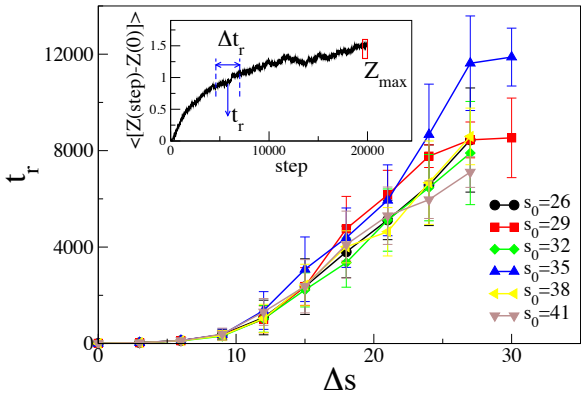

Figure 4.5. Relaxation time t_r of a bead s as a function of its position from the active site $\Delta s = s - s_0$. The relaxation time is calculated from the trajectories shown in Figure 4.3 as described in the text. Different symbols indicate different beads s_0 at the active site, as indicated in the legend. Inset figure shows the definitions of t_r, Δt_r and $Z_{\max}$ for a sample trajectory.

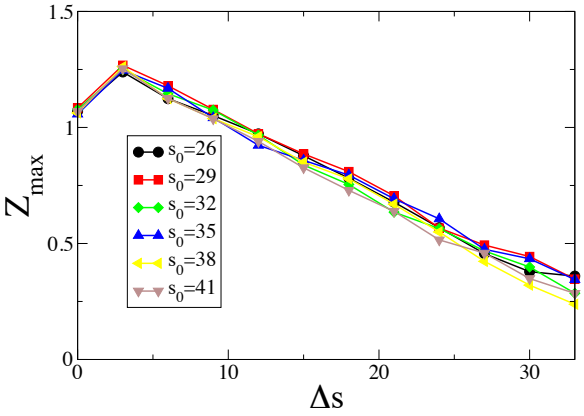

Figure 4.6. Characteristic displacement $Z_{\max}$ of a bead as a function of its relative position Δs. Different symbols indicate different beads present at the active site, as indicated in the legend.

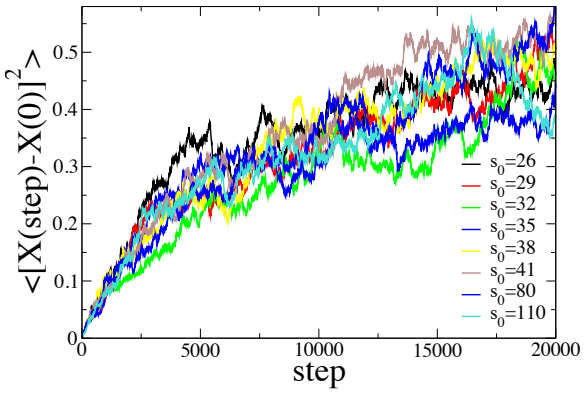

Figure 4.7. Mean square displacement in x-direction for beads near the interrogation point. Different colors indicate different beads s_0 at the active site, as indicated in the legend. The mean square displacement in x-direction begins to saturate at longer times.

In order to quantify these observations, we analyze the trajectories in terms of the maximum displacement of bead s of the ss-DNA in the z-direction and a characteristic time associated with its displacement. We define the maximum displacement $Z_{\max}$ of bead s as the average displacement that the bead undergoes in the last 500 steps of its trajectory, between steps 19501 and 20000 (inset of Figure 4.5). The characteristic relaxation time for a bead t_r is calculated as the time at which the bead undergoes characteristic displacement, which is defined as $(1-1/e)\times Z_{\max}$. Additionally, we also assign a width Δt_r to the displacement vs. time data, defined as half of the difference between the time taken for $\pm 10\%$ of the characteristic displacements. Inset of Figure 4.5 shows the definitions of these quantities for a sample trajectory. Figure 4.5 shows the variation of the characteristic relaxation time of subsequent beads s for different beads s_0 at the active site. The error bars indicate the corresponding values of Δt_r. For a given bead s, the characteristic relaxation time t_r is observed to increase as its relative position from the active site, denoted by $\Delta s = s - s_0$, increases. The disturbance introduced at the active site travels along the backbone of the ss-DNA as a wave. The amplitude of this wave decreases with distance from the active site, as seen from Figure 4.6.

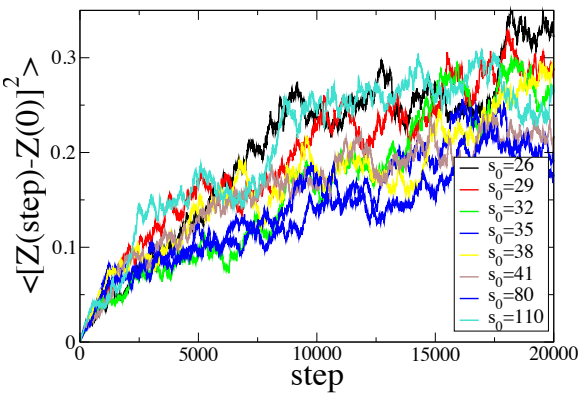

Figure 4.8. Mean square displacement in z-direction for beads near the interrogation point. Different colors indicate different beads s_0 at the active site, as indicated in the legend.

In translocation experiments, the narrowest region of the nanopore is termed as the interrogation point. For MspA nanopore, the interrogation point is identified at $z = -27.488$ in the current simulations. The square of the displacement of a DNA bead located nearest to the interrogation point during the pulling stage is monitored for each simulation run. Figure 4.7 shows the x-directional mean square displacement of beads located at the interrogation point for different values of s_0, averaged over all simulation runs. Figure 4.8 shows a similar plot for displacement in the z-direction. Due to computational constraints, we do not compute the mean square displacements beyond 20000 steps. However, the mean square displacement in both x- and z-directions appears to be saturating at longer times. The saturation in x-direction can be understood as a result of the confinement in x-direction due to the presence of the nanopore. No significant confinement is present in the z-direction due to the nanopore. However, the chain connectivity of the DNA along with the fixed position of bead s_0 at the active site ($z = 7.818$) can result into a saturation in the mean square displacement.

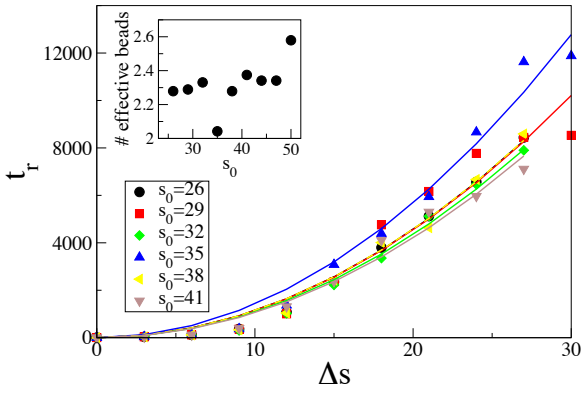

Figure 4.9. Fitting the Rouse relaxation time given by Equation 4.10 to the simulation results, for $t_{\text{relax}} = 10^6$. Symbols indicate the simulation data, while solid lines show the model result. Different colors show results for different beads present at the active site, as indicated in the legend.

4.4 Discussion

In reduced units, the Rouse time for a polymer of N segments, with each segment having a length of l reduced units, is given by the equation

$$\tau_{\text{Rouse}} = \frac{\zeta(Nl)^2}{12\pi^2}. \tag{4.7}$$

The bead friction coefficient $\zeta = 50.5$ and the bond length $l = 0.833$ are the same as the corresponding values used in the simulations. In simulations, we model the DNA chain using a three bead model for each nucleotide, with alternating sugar and phosphate beads along the backbone and a pendant base bead for each nucleotide. To map this to a linear Rouse chain, we define the parameter b as effective number of beads of equivalent friction that corresponds to a single unit in a linear chain of the same contour length as the DNA backbone. Using the effective number of beads, we define

$$\Delta\tilde{s} = \frac{\Delta s}{b}. \tag{4.8}$$

Using this definition, we obtain an expression for the Rouse time as

$$\tau_{\text{Rouse}} = \frac{\zeta l^2}{12\pi^2} \left[\Delta \tilde{s}\right]^2 . \tag{4.9}$$

We fit the simulation data with the quadratic equation of the form

$$\tau = a\Delta s^2 = ab^2[\Delta \tilde{s}]^2 \tag{4.10}$$

using the a as the fitting parameter. Comparing τ with τ_{Rouse} gives an expression for the effective number of beads b in terms of the fitting parameter a, as

$$b = \sqrt{\frac{\zeta l^2}{12\pi^2 a}}. \tag{4.11}$$

We perform the fitting using the least squares method, only including the data points for beads ($s < 80$) that have amplitude $Z_{\max} > 0.4$. Figure 4.9 shows the comparison of the simulation data and the equation, with the resulting values of effective number of beads shown in the inset. We observe that the effective number of beads is approximately equal to 2.3. This comparison suggests that the dynamics of the DNA chain inside the nanopore is not far from the Rouse dynamics.

4.5 Summary

Even for the simulated speed of the motor protein, which is much faster than experimentally observed speed of 40 nucleotides per second for the phi29 polymerase, the conformational fluctuations of DNA present inside the nanopore are not suppressed. Fluctuations of the DNA chain near the interrogation point (the region with the highest resistance towards small ion transport) primarily contribute to the noise in the blockade level in the ionic current trace. As discussed in Chapter 1, a low level of noise is desired to facilitate the detection of nucleotide sequence in a DNA. The findings of this work suggest that at the operating speeds of the phi29 polymerase,

the tension acting along the DNA chain due to the motor protein and the electric field acting in opposite directions is not enough to suppress the conformational fluctuations of the DNA.

CHAPTER 5

CONCLUSIONS AND FUTURE WORK

5.1 Conclusions

In this thesis, we have explored important aspects of polymer translocation through a nanopore. We have performed a detailed investigation of the effect of charge interactions between the nanopore and the polyelectrolyte. We have used Langevin dynamics simulations to study the effect of patterns of charges along the nanopore and the polyelectrolyte chain on kinetics of translocation. In the case of a uniformly charged polyelectrolyte chain translocating through a patterned nanopore, we have found that even when the total charge inside the nanopore remains the same, the distribution of the charge in patterns of alternating charged and uncharged sections leads to a non-monotonic dependence on the number of such sections, with a maximum corresponding to the largest mean translocation time. We have used a free energy landscape along the translocation coordinate that captures the underlying physics of the translocation process and using the free energy landscape we are able to map the translocation process to a 1-dimensional drift-diffusion equation based on the Fokker-Planck formalism. Our model is able to capture the non-monotonic dependence of translocation kinetics on charge patterns along the nanopore, with a single phenomenological constant that is independent of the patterns and the dimensions of the nanopore and the polyelectrolyte. The free energy landscape has helped us identify a free energy well located towards the end of translocation, when the polyelectrolyte chain is emptying the nanopore. The slowest translocation is a direct result of the steepest free energy well for the specific charge pattern along the

nanopore. We have also studied the case of a patterned polyelectrolyte chain translocating through a patterned nanopore. A pattern matching behavior is evident from our simulation results; the mean translocation time is sensitive to both the patterns and is the longest for a specific set of charge patterns along the nanopore and the polyelectrolyte chain. We have developed the underlying free energy landscape that shows features that can delay the translocation process not just during the nanopore emptying stage (as observed in the case of a uniformly charged polyelectrolyte), but also during the nanopore filling and the threading stage. Our simulations show that even the mean time for the threading stage is slowed down significantly due to the delay. This is an promising result in the context of polyelectrolyte characterization using nanopores, showing that the desired control over kinetics of translocation can be achieved by manipulating the tunable pore-polymer interactions..

We have studied the effect of polyelectrolyte architecture on the kinetics of its translocation through uncharged nanopores. Specifically, we have used Langevin dynamics simulations to study the kinetics of translocation of uniformly charged star polymers of varying number of arms. We have found that the number of arms of the star polymer, the star functionality, affect the translocation kinetics significantly and that the mean translocation time is a non-monotonic function of the functionality, with the fastest translocation observed for a critical functionality. We have performed a detailed parametric study to show that star polymers beyond a cutoff functionality do not translocate through narrow nanopores. The critical functionality and the cutoff functionality are shown to be sensitive to the nanopore dimensions. Our results are very exciting and demonstrate a promising approach towards using nanopores for characterizing charged polymers of various architectures using nanopores. Our simulation results have also helped in gaining insights into transport of star polymers. We have shown that star polymers predominantly translocate by dragging arms to-

wards the branch point and that the widely debated arm retraction mechanism is not observed.

Furthermore, we have studied the role of polyelectrolyte chain fluctuations inside the nanopore using Langevin dynamics simulations. We have simulated a construct consisting of opposing forces from a pulling motor (phi29 polymerase) and the electric field, which has been used in recent experiments to control the rate of translocation of polyelectrolytes (DNA) through an α-Hemolysin nanopore. We have used the power-stroke model to simulate the pulling motor protein and have used the displacement of the polyelectrolyte chain inside the nanopore to compute the relaxation time spectrum for chain segments of varying length. We have modeled the relaxation spectrum using predictions of the Rouse model for polymer dynamics. We have also measured the fluctuations of the polyelectrolyte chain at the interrogation point of the nanopore and have shown that these fluctuations, which are the primary source of noise in the experimentally measured ionic current signal, cannot be suppressed using the proposed construct.

Additionally, we have characterized the timescales involved in the translocation process using Langevin dynamics simulations and have identified the regime where the quasi-equilibrium assumption made in modeling translocation is valid. We have performed detailed simulations, incorporating hydrodynamics and long-range electrostatics, to measure the degree of ionization of a polyelectrolyte as it translocates through a nanopore.

5.2 Future work

Based on the understanding developed in this thesis, we would like to propose the following research tasks for future research directions.

5.2.1 Theory

The ability to describe the quasi-equilibrium process of translocation of a uniformly charged polymer translocating through a pore with charge decorations using the Fokker-Planck description has been one of the important findings of this work. In this thesis, a single phenomenological parameter k_0 is used as a fitting parameter to the model. Direct experimental measurement of this parameter or the related monomer friction coefficient is difficult. However, one can estimate the friction coefficient of a monomer under confinement from theoretical arguments. Solutions based on the Stokes-Einstein result for the mobility of a charged sphere in a solution have been proposed in the literature [94,95], with further improvements to incorporate confinement effects (see Ref. [96] for a detailed discussion). Attempts have been made to extend this to the case of a polymer under confinement, for example, in Ref. [97] . This can be further extended to the case of a polyelectrolyte chain under confinement to estimate the monomer friction coefficient from first principles, to improve the existing Fokker-Planck model.

5.2.2 Simulations

The effective charge of a translocating DNA is lower than its chemical valency due to counter-ion condensation that is further suppressed in presence of confinement. Estimating the effective charge is difficult from experiments, but can be easily obtained from simulations. In this thesis, we have made a quick estimate of the degree of counter-ion condensation for the case of an uncharged nanopore. Obtaining such an estimate for the more realistic situations of (a) a uniformly charged solid-state nanopore and (b) a charge decorated protein nanopore is required to complement the rich experimental data available in the literature on translocation kinetics of polyelectrolytes through these nanopores. An accurate estimation of the effective charge for these situations can be obtained using the simulation technique used in

this thesis. However, the effect of dielectric mismatch between the membrane and the bulk must be incorporated into the simulation. The method of image charges can be implemented using the iterative scheme proposed in Ref. [98] to incorporate dielectric mismatch. Such a simulation setup can also be used to characterize the electro-osmotic flow inside the nanopore due to charges along the nanopore surface and to estimate the ionic current traces during translocation. Estimation of these quantities is of immediate interest since it is crucial in improving our current state of understanding the translocation phenomenon.

APPENDICES

APPENDIX A

LANGEVIN DYNAMICS SIMULATIONS

Simulation details

The system is made up of three components: an uncharged membrane, a cylindrical pore inside the membrane, and a charged polymer chain. Details of each of these components are described below, with all quantities in reduced units, unless specified otherwise.

The membrane is M unit thick, and has a cylindrical pore of radius r_p. The membrane walls are modelled using spherical beads of diameter $d_1 = 1$ arranged into a two dimensional grid with grid-spacing of d_1. The pore wall is made up of smaller beads of diameter d_2, with the ratio $d_2/d_1 = 0.25$. These beads are placed along the circumference of a cylinder, with each bead approximately at a distance of $d_2/2$ from each other. This overlapping of pore wall beads is done to make the pore cross-section more circular. A part of membrane walls surrounding both ends of the pore is made up of beads identical to the pore wall beads. N beads of diameter d_1 are connected by harmonic bonds to form a uniform polymer. The equilibrium bond length is taken to be equal to d_1. A unit negative charge is placed on each polymer bead.

Pair-wise interactions

Excluded volume interactions are modelled using a truncated Lennard-Jones potential between two beads, given by the equation,

$$U_{\mathrm{LJ}} = \begin{cases} 4\epsilon_{\mathrm{LJ}} \left[\left(\frac{\sigma}{r}\right)^{12} - \left(\frac{\sigma}{r}\right)^{6} \right] + \epsilon_{\mathrm{LJ}} & \text{for } r \leq 1.12\sigma \\ 0 & \text{for } r > 1.12\sigma. \end{cases} \tag{A.1}$$

Here, r is the distance between two beads. $\epsilon_{\mathrm{LJ}} = 1$ (≈ 0.1 Kcal/mol) is the depth of the potential well, with $T = 300$ K. The potential is truncated at its minimum, corresponding to a distance of 1.12σ. These interactions exist between all the beads, with $\sigma = 1$ for interactions between polymer-polymer and polymer-membrane beads, and $\sigma = 0.625$ for pore-polymer beads. Since the positions of pore and membrane beads are fixed in the simulation, pair-wise interactions are not computed for these beads.

Electrostatic interactions between a pair of beads are modelled using the truncated Debye-Hückel potential, with an inverse of the Debye length κ corresponding to a monovalent salt concentration of 0.1M,

$$U_{\mathrm{DH}} = \frac{C q_i q_j}{\epsilon} \frac{\exp(-\kappa r)}{r} \qquad \text{for } r \leq r_{c2} \tag{A.2}$$

with q_i and q_j corresponding to the charges on beads i and j, separated by a distance r. Although the effective dielectric constant of an electrolyte solution confined within a nanopore is unknown, we have taken $\epsilon = 80$. r_{c2} is the cutoff distance at which the electrostatic interactions are truncated. A value of $r_{c2} = 3$ is used in all the simulations.

Pair-wise electrostatic interactions are computed between polymer-polymer beads and pore-polymer beads. For polymer-polymer electrostatic interactions, $q_1 = q_2 = -1e$ ($e = 1.60217646 \times 10^{-19}$ Coulomb is the elementary charge). The pore-polymer electrostatic interactions are computed using $q_1 = -1e$ and $q_2 = \alpha_p e$ for pore beads belonging to a charged section. As described in reference [52], the energy conversion constant $C = 1$ in the present units.

The bonds between polymer beads are modelled using a harmonic potential. The equilibrium bond length between two connected polymer beads is $r_0 = 1$. The value of spring constant $K = 15480$ (≈ 10 Kcal/(mol Å^2)) is large enough to prevent unrealistic bond extensions.

$$U_b = K(r - r_0)^2 \tag{A.3}$$

In Langevin dynamics simulation, the above potentials are used to compute forces on each of the polymer beads. The equation of motion for each bead is given by

$$m\frac{d^2r}{dt^2} = -\zeta\frac{dr}{dt} - \nabla(U_{\mathrm{LJ}} + U_{\mathrm{DH}} + U_b) + F_r + F_{\mathrm{ext}} \tag{A.4}$$

where m is mass of the bead, ζ is the friction coefficient, and $F_r \sim \sqrt{k_B T\zeta/dt}$ is the random force due to solvent at the given temperature T, as documented extensively in the literature [52]. We choose the values $m = 1$ and $\zeta = 1$ in all our simulations. The force due to applied electric field E acting on each bead is given by $F_{\mathrm{ext}} = q_1 E$.

APPENDIX B

MOLECULAR DYNAMICS SIMULATIONS

Simulation details

The system is made of three components, an uncharged membrane embedded with a cylindrical pore, a charged polymer chain and small ions that consist of counter-ions and salt ions. Details of each of these components are described below, with all quantities in reduced units unless specified otherwise.

The polymer chain and the small ions are represented using spherical beads. Each bead has an excluded volume that is modeled by truncated Lennard-Jones potential given by Equation A.1, with $\sigma = 1$ and $\epsilon_{\mathrm{LJ}} = 1$. The N polymer beads representing the polymer chain backbone are connected linearly using harmonic bonds that are represented by Equation A.3, with the equilibrium bond length $r_0 = 1$ and the spring constant $K = 5000$. The polymer beads hold a unit negative charge, with equal number of small ions bearing a unit positive charge. One half of the remainder number of small ions (corresponding to a specified salt concentration) bear a unit positive charge and the other half bear a unit negative charge (monovalent salt ions). Charge interactions are modeled using the Coulomb potential given as follows.

$$U_{\mathrm{charge}} = \frac{1}{4\pi\epsilon\epsilon_0}\frac{q_i q_j}{r} \tag{B.1}$$

with q_i and q_j corresponding to the charges on beads i and j, separated by a distance r. For implementing this long-range potential in our simulations (consisting of periodic boundaries), the particle-particle-particle-mesh method is used (see Ref. [55, 99]). Essentially, the method comprises of splitting the total potential into a short-range

particle-particle interaction potential and a long-range interaction potential solved on a mesh using fast Fourier transformation, providing a faster convergence in calculating the sum of the Coulomb potential for all particles and their images accurately. The input parameters for this method are the desired accuracy for the calculation, the cutoff distance to split the potential, and number of neighboring grid points on the mesh used for interpolation scheme used for mapping particles onto the mesh. The desired accuracy is chosen to be 10^{-4}, while the cutoff distance is 5 and 7 points are used in the interpolation scheme.

The membrane divides the simulation box into two compartments that are connected via a cylindrical nanopore of length M and radius r_p. The two vertical surfaces of the membrane and the cylindrical surface of the nanopore have an excluded volume modeled by the truncated Lennard-Jones potential with same parameters as for the polymer and the small ions. For computational efficiency, these beads are implemented as ghost beads that are not present until a polymer or small ion bead approaches the surface.

Each bead undergoes molecular dynamics represented by the following equation of motion.

$$m\frac{d^2r}{dt^2} = -\nabla(U_{\mathrm{LJ}} + U_{\mathrm{charge}} + U_{\mathrm{b}}) + F_{\mathrm{ext}} \tag{B.2}$$

where m is mass of the bead, and the force due to applied electric field E acting on ith bead inside the nanopore is given by $F_{\mathrm{ext}} = q_i E$.

The equation of motion is integrated using the velocity-Verlet algorithm with a time-step of 0.005. Additionally, after every 0.1 time-steps, the bead velocities are updated according to the multi-particle collision dynamics equation discussed next.

Multi-particle collision dynamics

Hydrodynamics is implemented using the particle based method: multi-particle collision dynamics [54, 100–102]. The input parameters to this model are the particle

density, rotation angle (θ) and time-step (h). The simulation box is divided into cubic cells with unit length of side. The average particle density in each cell is 10, with particle positions and velocities assigned randomly (corresponding to unit temperature) and these particles evolve as they undergo two steps: streaming and collision. In the streaming step, the particle positions r_i are updated as per their instantaneous velocities $v_i(t)$ for a time-step $h = 0.1$.

$$r_i(t+h) = r_i(t) + h \times v_i(t) \tag{B.3}$$

A no-slip boundary condition is implemented using the bounce back rule for particles at the surface of the membrane or the nanopore.

$$v_i(t_c) = -v_i(t_c) \qquad \text{at boundary} \tag{B.4}$$

where t_c is the time instant at which collision with surface occurs. In the collision step, particle velocities are rotated with the rotation rule,

$$v_i^{\text{new}}(t+h) = v_i(t+h) + (R(\theta) - I)(v_i(t+h) - v_{\text{cm}}(t+h) \tag{B.5}$$

where $v_{\text{cm}}(t+h)$ is the instantaneous center-of-mass velocity of the cell that the particle belongs to, $R(\theta)$ is the rotation matrix corresponding to the rotation angle θ along a randomly chosen axis [103], and $v_i^{\text{new}}(t+h)$ is the new velocity assigned to the particle. The solute beads (polymer and small ion beads) interact with the hydrodynamic particles through this rotation step. Thus, the solvent bead velocities are rotated after time h along with the hydrodynamic particles. The center-of-mass velocity of jth cell is computed as,

$$v_{\text{cm}}(t) = \frac{1}{N_j + 10N_s} \left[\sum_{i=1}^{N_j} v_i(t) + \sum_{i=1}^{N_s} 10V_i(t) \right] \tag{B.6}$$

Here, N_j is the number of hydrodynamic particles belonging to the jth cell, and N_s is the number of solute beads belonging to that cell. $V_i(t)$ is the velocity of ith solute bead. To improve the method further, the random shift technique proposed in Ref. [102] is implemented: the origin used to define the cells is randomly shifted within a unit distance at every collision step.

BIBLIOGRAPHY

[1] Kasianowicz, J. J., Brandin, E., Branton, D., and Deamer, D. W. "Characterization of individual polynucleotide molecules using a membrane channel". *P. Natl. Acad. Sci. U.S.A.*, **93**, 24, 13770–13773 (1996).

[2] Chen, X., Rungger, I., Pemmaraju, C. D., Schwingenschloegl, U., and Sanvito, S. "First-principles study of high-conductance DNA sequencing with carbon nanotube electrodes". *Phys. Rev. B*, **85**, 11, 115436 (2012).

[3] Cherf, G. M., Lieberman, K. R., Rashid, H., Lam, C. E., Karplus, K., and Akeson, M. "Automated forward and reverse ratcheting of DNA in a nanopore at 5-Å precision". *Nat. Biotechnol.*, **30**, 4, 344–348 (2012).

[4] Manrao, E. A., Derrington, I. M., Laszlo, A. H., Langford, K. W., Hopper, M. K., Gillgren, N., Pavlenok, M., Niederweis, M., and Gundlach, J. H. "Reading DNA at single-nucleotide resolution with a mutant MspA nanopore and phi29 DNA polymerase". *Nat. Biotechnol.*, **30**, 4, 349–353 (2012).

[5] Wanunu, M., Sutin, J., McNally, B., Chow, A., and Meller, A. "DNA translocation governed by interactions with solid-state nanopores". *Biophys. J.*, **95**, 10, 4716–4725 (2008).

[6] Chen, P., Gu, J., Brandin, E., Kim, Y.-R., Wang, Q., and Branton, D. "Probing single DNA molecule transport using fabricated nanopores". *Nano Lett.*, **4**, 11, 2293–2298 (2004).

[7] Kowalczyk, S. W., Wells, D. B., Aksimentiev, A., and Dekker, C. "Slowing down DNA translocation through a nanopore in lithium chloride". *Nano Lett.*, **12**, 2, 1038–1044 (2012).

[8] Alberts, B., Johnson, A., Lewis, J., Raff, M., Roberts, K., and Walter, P. *Molecular Biology of the Cell*. Garland Science, fourth edition (2002).

[9] Li, J., Gershow, M., Stein, D., Brandin, E., and Golovchenko, J. A. "DNA molecules and configurations in a solid-state nanopore microscope". *Nat. Mater.*, **2**, 9, 611–615 (2003).

[10] Storm, A. J., Chen, J. H., Ling, X. S., Zandbergen, H. W., and Dekker, C. "Fabrication of solid-state nanopores with single-nanometre precision". *Nat. Mater.*, **2**, 8, 537–540 (2003).

[11] Muthukumar, M. *Polymer Translocation*. CRC Press (2011).

[12] Wong, C. T. A. and Muthukumar, M. "Polymer translocation through α-hemolysin pore with tunable polymer-pore electrostatic interaction". *J. Chem. Phys.*, **133**, 4, 045101 (2010).

[13] Jeon, B.-j. and Muthukumar, M. "Polymer capture by α-hemolysin pore upon salt concentration gradient". *J. Chem. Phys.*, **140**, 1, 015101 (2014).

[14] Cohen, J. A., Chaudhuri, A., and Golestanian, R. "Stochastic sensing of polynucleotides using patterned nanopores". *Phys. Rev. X*, **2**, 2, 021002 (2012).

[15] Katkar, H. H. and Muthukumar, M. "Effect of charge patterns along a solid-state nanopore on polyelectrolyte translocation". *J. Chem. Phys.*, **140**, 13, 135102 (2014).

[16] Saito, T. and Sakaue, T. "Process time distribution of driven polymer transport". *Phys. Rev. E*, **85**, 6, 061803 (2012).

[17] Sarabadani, J., Ikonen, T., and Ala-Nissila, T. "Iso-flux tension propagation theory of driven polymer translocation: The role of initial configurations". *J. Chem. Phys.*, **141**, 21, 214907 (2014).

[18] Sung, W. and Park, P. J. "Polymer translocation through a pore in a membrane". *Phys. Rev. Lett.*, **77**, 4, 783–786 (1996).

[19] Muthukumar, M. "Polymer translocation through a hole". *J. Chem. Phys.*, **111**, 22, 10371–10374 (1999).

[20] Polson, J. M. and McCaffrey, A. C. M. "Polymer translocation dynamics in the quasi-static limit". *J. Chem. Phys.*, **138**, 17, 174902 (2013).

[21] Kantor, Y. and Kardar, M. "Anomalous dynamics of forced translocation". *Phys. Rev. E*, **69**, 2, 021806 (2004).

[22] de Haan, H. W. and Slater, G. W. "Translocation of a polymer through a nanopore across a viscosity gradient". *Phys. Rev. E*, **87**, 4, 042604 (2013).

[23] Luo, K., Huopaniemi, I., Ala-Nissila, T., and Ying, S.-C. "Polymer translocation through a nanopore under an applied external field". *J. Chem. Phys.*, **124**, 11, 114704 (2006).

[24] Wong, C. T. A. and Muthukumar, M. "Polymer capture by electro-osmotic flow of oppositely charged nanopores". *J. Chem. Phys.*, **126**, 16, 164903 (2007).

[25] Kong, C. Y. and Muthukumar, M. "Modeling of polynucleotide translocation through protein pores and nanotubes". *Electrophoresis*, **23**, 16, 2697–2703 (2002).

[26] Muthukumar, M. and Kong, C. Y. "Simulation of polymer translocation through protein channels". *P. Natl. Acad. Sci. U.S.A.*, **103**, 14, 5273–5278 (2006).

[27] Wanunu, M., Morrison, W., Rabin, Y., Grosberg, A. Y., and Meller, A. "Electrostatic focusing of unlabelled DNA into nanoscale pores using a salt gradient". *Nat. Nanotechnol.*, **5**, 2, 160–165 (2009).

[28] Muthukumar, M. "Polymer escape through a nanopore". *J. Chem. Phys.*, **118**, 11, 5174–5184 (2003).

[29] Forrey, C. and Muthukumar, M. "Langevin dynamics simulations of ds-DNA translocation through synthetic nanopores". *J. Chem. Phys.*, **127**, 1, 015102 (2007).

[30] Maglia, G., Restrepo, M. R., Mikhailova, E., and Bayley, H. "Enhanced translocation of single DNA molecules through α-hemolysin nanopores by manipulation of internal charge". *P. Natl. Acad. Sci. U.S.A.*, **105**, 50, 19720–19725 (2008).

[31] Anderson, B. N., Muthukumar, M., and Meller, A. "pH tuning of DNA translocation time through organically functionalized nanopores". *ACS Nano*, **7**, 2, 1408–1414 (2013).

[32] Muthukumar, M. "Theory of sequence effects on DNA translocation through proteins and nanopores". *Electrophoresis*, **23**, 10, 1417–1420 (2002).

[33] Mirigian, S., Wang, Y., and Muthukumar, M. "Translocation of a heterogeneous polymer". *J. Chem. Phys.*, **137**, 6, 064904 (2012).

[34] Jeon, B.-j. and Muthukumar, M. "Determination of molecular weights in polyelectrolyte mixtures using polymer translocation through a protein nanopore". *ACS Macro Lett.*, **3**, 9, 911–915 (2014).

[35] Brun, L., Pastoriza-Gallego, M., Oukhaled, G., Mathé, J., Bacri, L., Auvray, L., and Pelta, J. "Dynamics of polyelectrolyte transport through a protein channel as a function of applied voltage". *Phys. Rev. Lett.*, **100**, 15, 158302 (2008).

[36] Murphy, R. J. and Muthukumar, M. "Threading synthetic polyelectrolytes through protein pores". *J. Chem. Phys.*, **126**, 5, 051101 (2007).

[37] Meller, A., Nivon, L., Brandin, E., Golovchenko, J., and Branton, D. "Rapid nanopore discrimination between single polynucleotide molecules". *P. Natl. Acad. Sci. U.S.A.*, **97**, 3, 1079–1084 (2000).

[38] Meller, A., Nivon, L., and Branton, D. "Voltage-driven DNA translocations through a nanopore". *Phys. Rev. Lett.*, **86**, 15, 3435–3438 (2001).

[39] Eisenriegler, E. "Adsorption of polymer chains at surfaces: Scaling and Monte Carlo analyses". *J. Chem. Phys.*, **77**, 12, 6296 (1982).

[40] Muthukumar, M. and Katkar, H. "Reading nanopore clocks in single-molecule electrophoresis experiments". *Biophys. J.*, **108**, 1, 1719 (2015).

[41] Sakaue, T. "Nonequilibrium dynamics of polymer translocation and straightening". *Phys. Rev. E*, **76**, 2, 021803 (2007).

[42] Sakaue, T. "Sucking genes into pores: Insight into driven translocation". *Phys. Rev. E*, **81**, 4, 041808 (2010).

[43] Rowghanian, P. and Grosberg, A. Y. "Force-driven polymer translocation through a nanopore: An old problem revisited". *J. Phys. Chem. B*, **115**, 48, 14127–14135 (2011).

[44] Rowghanian, P. and Grosberg, A. Y. "Propagation of tension along a polymer chain". *Phys. Rev. E*, **86**, 1, 011803 (2012).

[45] Saito, T. and Sakaue, T. "Dynamical diagram and scaling in polymer driven translocation". *Eur. Phys. J. E*, **34**, 12, 135 (2011).

[46] Saito, T. and Sakaue, T. "Erratum to: Dynamical diagram and scaling in polymer driven translocation". *Eur. Phys. J. E*, **35**, 11, 125 (2012).

[47] Ikonen, T., Bhattacharya, A., Ala-Nissila, T., and Sung, W. "Unifying model of driven polymer translocation". *Phys. Rev. E*, **85**, 5, 051803 (2012).

[48] Ikonen, T., Bhattacharya, A., Ala-Nissila, T., and Sung, W. "Influence of non-universal effects on dynamical scaling in driven polymer translocation". *J. Chem. Phys.*, **137**, 8, 085101 (2012).

[49] Ikonen, T., Bhattacharya, A., Ala-Nissila, T., and Sung, W. "Influence of pore friction on the universal aspects of driven polymer translocation". *Europhys. Lett.*, **103**, 3, 38001 (2013).

[50] Adhikari, R. and Bhattacharya, A. "Driven translocation of a semi-flexible chain through a nanopore: A Brownian dynamics simulation study in two dimensions". *J. Chem. Phys.*, **138**, 20, 204909 (2013).

[51] Bhattacharya, A. "Translocation dynamics of a semiflexible chain under a bias: Comparison with tension propagation theory". *Polym. Sci., Ser. C*, **55**, 1, 60–69 (2013).

[52] Plimpton, S. "Fast parallel algorithms for short-range molecular dynamics". *J. Comp. Phys.*, **117**, 1, 1–19 (1995).

[53] Hoogerheide, D. P., Albertorio, F., and Golovchenko, J. A. "Escape of DNA from a weakly biased thin nanopore: Experimental evidence for a universal diffusive behavior". *Phys. Rev. Lett.*, **111**, 24, 248301 (2013).

[54] Singh, S. P. and Muthukumar, M. "Electrophoretic mobilities of counterions and a polymer in cylindrical pores". *J. Chem. Phys.*, **141**, 11, 114901 (2014).

[55] Hockney, R. and Eastwood, J. *Computer Simulation Using Particles*. Advanced book program: Addison-Wesley. McGraw-Hill (1981).

[56] Luo, K., Ala-Nissila, T., Ying, S.-C., and Bhattacharya, A. "Influence of polymer-pore interactions on translocation". *Phys. Rev. Lett.*, **99**, 14, 148102 (2007).

[57] Luan, B., Stolovitzky, G., and Martyna, G. "Slowing and controlling the translocation of DNA in a solid-state nanopore". *Nanoscale*, **4**, 4, 1068–1077 (2012).

[58] Lu, B., Hoogerheide, D. P., Zhao, Q., and Yu, D. "Effective driving force applied on DNA inside a solid-state nanopore". *Phys. Rev. E*, **86**, 1, 011921 (2012).

[59] Ding, K., Yan, Q., Wang, N., Wu, F., and Wu, Z. "Surface-charge effects on the movement of a polyelectrolyte through a solid-state nanopore". *Eur. Phys. J.-Appl. Phys.*, **58**, 3, 31201 (2012).

[60] Rasmussen, C. J., Vishnyakov, A., and Neimark, A. V. "Translocation dynamics of freely jointed Lennard-Jones chains into adsorbing pores". *J. Chem. Phys.*, **137**, 14, 144903 (2012).

[61] He, Y., Tsutsui, M., Taniguchi, M., and Kawai, T. "DNA capture in nanopores for genome sequencing: challenges and opportunities". *J. Mater. Chem.*, **22**, 27, 13423–13427 (2012).

[62] Luo, K., Ala-Nissila, T., Ying, S.-C., and Bhattacharya, A. "Heteropolymer translocation through nanopores". *J. Chem. Phys.*, **126**, 14, 145101 (2007).

[63] Gauthier, M. G. and Slater, G. W. "Sequence effects on the forced translocation of heteropolymers through a small channel". *J. Chem. Phys.*, **128**, 17, 175103 (2008).

[64] Gardiner, C. W. *Handbook of Stochastic Methods for Physics, Chemistry, and the Natural Sciences*. Berlin: Springer-Verlag, second edition (1985).

[65] Cox, D. R. and Miller, H. D. *The Theory of Stochastic Processes*. New York: Wiley (1968).

[66] Grest, G. S., Fetters, L. J., Huang, J. S., and Richter, D. "Star polymers: Experiment, theory, and simulation". *Adv. Chem. Phys.*, **94**, 67–163 (1996).

[67] Volkmuth, W. D., Duke, T., Austin, R. H., and Cox, E. C. "Trapping of branched DNA in microfabricated structures". *P. Natl. Acad. Sci. U.S.A.*, **92**, 15, 6887–6891 (1995).

[68] Bell, L. and Byers, B. "Separation of branched from linear DNA by two-dimensional gel electrophoresis". *Anal. Biochem.*, **130**, 2, 527–535 (1983).

[69] Xing, J., Tan, L., Cao, F., and Wang, Y. "Synthesis of star polymer poly(ethylene glycol)3poly(n,n-dimethyl acrylamide) and its application in protein resistance and separation". *J. Appl. Polym. Sci.*, **129**, 3, 1179–1186 (2013).

[70] Heuer, D. M., Saha, S., and Archer, L. A. "Electrophoretic dynamics of large DNA stars in polymer solutions and gels". *Electrophoresis*, **24**, 19-20, 3314–3322 (2003).

[71] Saha, S., Heuer, D. M., and Archer, L. A. "Electrophoretic mobility of linear and star-branched DNA in semidilute polymer solutions". *Electrophoresis*, **27**, 16, 3181–3194 (2006).

[72] Hoffmann, I., de Molina, P. M., Farago, B., Falus, P., Herfurth, C., Laschewsky, A., and Gradzielski, M. "Dynamics of microemulsions bridged with hydrophobically end-capped star polymers studied by neutron spin-echo". *J. Chem. Phys.*, **140**, 3, 034902 (2014).

[73] de Gennes, P. G. "Reptation of stars". *J. Phys. (Paris)*, **36**, 1199–1203 (1975).

[74] Graessley, W. W. "Entangled linear, branched and network polymer systems - molecular theories". *Adv. Polym. Sci.*, **47**, 67117 (1982).

[75] Doi, M. and Kuzuu, N. Y. "Rheology of star polymers in concentrated solutions and melts". *J. Polym. Sci. Polym. Lett. Ed.*, **18**, 12, 775–780 (1980).

[76] Klein, J., Fletcher, D., and Fetters, L. J. "Dynamics of entangled star-branched polymers". *Faraday Symp. Chem. Soc.*, **18**, 159–171 (1983).

[77] Pearson, D. S. and Helfand, E. "Viscoelastic properties of star-shaped polymers". *Macromolecules*, **17**, 4, 888–895 (1984).

[78] Heuer, D. M., Saha, S., Kusumo, A. T., and Archer, L. A. "Influence of branch length asymmetry on the electrophoretic mobility of rigid rod-like DNA". *Electrophoresis*, **25**, 12, 1772–1783 (2004).

[79] Milchev, A., Müller, M., and Klushin, L. "Arm retraction dynamics and bistability of a three-arm star polymer in a nanopore". *Macromolecules*, **47**, 6, 2156–2168 (2014).

[80] Račko, D. and Cifra, P. "Arm retraction and escape transition in semi-flexible star polymer under cylindrical confinement". *J. Mol. Model.*, **21**, 7, 186 (2015).

[81] Brochard-Wyart, F. and de Gennes, P. G. "Injection threshold for a star polymer inside a nanopore". *C. R. Acad. Sci. Ser. II B*, **323**, 7, 473–479 (1996).

[82] de Gennes, P. G. "Polymers in confined environments". *Adv. Polym. Sci.*, **138**, 91–105 (1999).

[83] Li, Z., Li, Y., Wang, Y., Sun, Z., and An, L. "Transport of star-branched polymers in nanoscale pipe channels simulated with dissipative particle dynamics simulation". *Macromolecules*, **43**, 13, 5896–5903 (2010).

[84] Ripoll, M., Winkler, R. G., and Gompper, G. "Hydrodynamic screening of star polymers in shear flow". *Eur. Phys. J. E*, **23**, 4, 349–354 (2007).

[85] Hernández Cifre, J., López Martínez, M., and García de la Torre, J. "Conformation and dynamics of star-branched flexible polymer chains in a flowing solution". *J. Non-Cryst. Solids*, **307**, 818–823 (2002).

[86] Hernández Cifre, J., Pamies, R., López Martínez, M., and García de la Torre, J. "Steady-state behavior of star polymers in dilute flowing solutions via Brownian dynamics". *Polymer*, **46**, 18, 6756–6766 (2005).

[87] Liu, Z., Liu, J., Xiao, M., Wang, R., and Chen, Y.-L. "Conformation-dependent translocation of a star polymer through a nanochannel". *Biomicrofluidics*, **8**, 5, 054107 (2014).

[88] Ibarra, B., Chemla, Y. R., Plyasunov, S., Smith, S. B., Lzaro, J. M., Salas, M., and Bustamante, C. "Proofreading dynamics of a processive DNA polymerase". *EMBO J.*, **28**, 18, 2794–2802 (2009).

[89] Glick, B. S. "Can Hsp70 proteins act as force-generating motors?" *Cell*, **80**, 1, 11–14 (1995).

[90] Elston, T. C. "The brownian ratchet and power stroke models for posttranslational protein translocation into the endoplasmic reticulum". *Biophys. J.*, **82**, 3, 1239–1253 (2002).

[91] Berman, A. J., Kamtekar, S., Goodman, J. L., Lázaro, J. M., de Vega, M., Blanco, L., Salas, M., and Steitz, T. A. "Structures of phi29 DNA polymerase complexed with substrate: the mechanism of translocation in B-family polymerases". *EMBO J.*, **26**, 14, 3494–3505 (2007).

[92] Faller, M., Niederweis, M., and Schulz, G. E. "The structure of a Mycobacterial outer-membrane channel". *Science*, **303**, 5661, 1189–1192 (2004).

[93] Cussler, E. L. *Diffusion: Mass transfer in fluid systems*. Cambridge University Press (2000).

[94] Hückel, E. "The cataphoresis of the sphere". *Phys. Z.*, **25**, 204–210 (1924).

[95] Henry, D. C. "The cataphoresis of suspended particles. part I. the equation of cataphoresis". *Proc. R. Soc. London, Ser. A*, **133**, 821, 106129 (1931).

[96] Muthukumar, M. "Communication: Charge, diffusion, and mobility of proteins through nanopores". *J. Chem. Phys.*, **141**, 8, 081104 (2014).

[97] Harden, J. L. and Doi, M. "Diffusion of macromolecules in narrow capillaries". *J. Phys. Chem.*, **96**, 10, 4046–4052 (1992).

[98] Tyagi, S., Suzen, M., Sega, M., Barbosa, M., Kantorovich, S. S., and Holm, C. "An iterative, fast, linear-scaling method for computing induced charges on arbitrary dielectric boundaries". *J. Chem. Phys.*, **132**, 15, 154112 (2010).

[99] Deserno, M. and Holm, C. "How to mesh up Ewald sums. I. A theoretical and numerical comparison of various particle mesh routines". *J. Chem. Phys.*, **109**, 18, 7678 (1998).

[100] Malevanets, A. and Kapral, R. "Mesoscopic model for solvent dynamics". *J. Chem. Phys.*, **110**, 17, 8605 (1999).

[101] Malevanets, A. and Yeomans, J. M. "Dynamics of short polymer chains in solution". *Europhys. Lett.*, **52**, 2, 231–237 (2000).

[102] Ihle, T. and Kroll, D. M. "Stochastic rotation dynamics: A Galilean-invariant mesoscopic model for fluid flow". *Phys. Rev. E*, **63**, 2, 020201 (2001).

[103] Huang, C.-C., Gompper, G., and Winkler, R. G. "Hydrodynamic correlations in multiparticle collision dynamics fluids". *Phys. Rev. E*, **86**, 5, 056711 (2012).